The Thesis Committee for Sonia Arumdati Purba
Certifies that this is the approved version of the following thesis:

New Method for Rock Classification in Carbonate Formations using Well-Log-Based Rock Fabric Quantification

APPROVED BY
SUPERVISING COMMITTEE:

Supervisor:

Zoya Heidari

Carlos Torres-Verdin

New Method for Rock Classification in Carbonate Formations using Well-Log-Based Rock Fabric Quantification

by

Sonia Arumdati Purba

Thesis

Presented to the Faculty of the Graduate School of

The University of Texas at Austin

in Partial Fulfillment

of the Requirements

for the Degree of

Master of Science in Engineering

The University of Texas at Austin

December 2017

Dedication

To my family and the glory of Jesus Christ.

Acknowledgements

I would like to give thanks to God for His blessings and guidance for me in finishing this thesis. Thank you to my family for their support and prayers from the start of my program till now.

My heartfelt gratitude goes to my supervisor, Dr. Zoya Heidari for her patience in guiding me since my first day here. She has supported, guided, and inspired me to keep on pushing and moving towards the end of my M.S. program. It was an honor to have the chance to work with you. Also, thank you to Dr. Carlos Torres-Verdin, as a part of my reader committee, for his valuable comments, help, and grace he showed towards the process of finishing this thesis.

I also would like to express my sincere gratitude to Artur Posenato Garcia for his invaluable comments, mentorship, and kindness displayed to me. Thank you for not only performing the numerical simulations needed for my research but also for being my mentor from my first day here at The University of Texas at Austin. I am forever grateful for the mentorship you provided and for the friendship that we have. Special thanks to Emmanuel Oyewole for developing the permeability assessment workflow applied in this thesis and scanning several pore-scale rock samples. I am also grateful for Chelsea Newgord for her feedback on my thesis. I also would like to thank my friends in the Multi-Scale Rock Physics Group for the partnership in the past two years I am here. I wish only for your success in the years to come.

I would also like to acknowledge and express my gratitude to my sponsor, Lembaga Dana Pengelola Pendidikan, under Indonesia's Ministry of Finance, for providing me this amazing opportunity for my future career.

Finally, I would like to thank my Indonesian community here for being like a family to me here in Austin. Thank you to Barisan Sakit Hati, and especially to Yohanes Sitanggang, for the friendship that we have over the last two years.

Abstract

New Method for Rock Classification in Carbonate Formations using Well-Log-Based Rock Fabric Quantification

Sonia Arumdati Purba, M.S.E.

The University of Texas at Austin, 2017

Supervisor: Zoya Heidari

Challenges in rock classification of complex carbonate formations are often rooted in the failure to consider the spatial distribution of pore network or rock fabric. It is crucial to quantify rock fabric through different petrophysical properties that are affected by it. For example, Mercury Injection Capillary Pressure (MICP)-based pore typing uses the estimated pore-size distribution to cluster different pore types. Another example is well-log-based rock quality factor that takes advantage of the mud-filtrate invasion effects on well logs as proxy to the pore-size distribution. However, such methods require prior knowledge of the number of rock classes, which is mainly rooted in the differences between petrophysical rock classes and geological depositional facies. This thesis introduces a method for improving rock classification by determining the optimum number of rock classes, evaluating and quantifying pore network connectivity and geometry as rock fabric, as well as enhancing petrophysical evaluation.

The proposed method involves an iterative procedure that starts with conventional well-log interpretation to obtain the petrophysical properties, such as volumetric

concentration of shale, porosity, and permeability. Rock classification is performed using an unsupervised neural network with an initial assumption of the number of rock classes and well-log-based estimates of petrophysical and compositional properties as inputs. Permeability models are then developed in the pore-scale domain using core subsamples at different depths of interest. Models describing the correlation between electrical resistivity, conducting or effective porosity, and permeability are established in the pore-scale domain. These models are then applied in the log-scale domain to improve permeability estimates. Next, rock classification will be performed using the improved permeability estimates as inputs and updating number of rock classes. This process is repeated until a convergence in permeability estimates is achieved. outcomes of the iterative method include log-scale rock classification, permeability estimates, and the optimum number of rock classes.

The method introduced in this thesis was successfully applied to two wells in a carbonate formation. outcomes of rock classification are in good agreement with the geological depositional facies. The iterative method results in 75% improvement in permeability estimates in the log-scale domain when compared against those obtained from conventional porosity-permeability correlations. Furthermore, this method effectively optimizes the number of rock classes, making it a promising approach for field cases with limited core measurements and no prior knowledge of rock types.

Table of Contents

List of Tables

List of Figures

Chapter 1: Introduction and Literature Review

Lucia (2012) explains that reservoir characterization aims to describe the spatial distribution of petrophysical parameters such as porosity, permeability, and saturation. Therefore, rock classification is fundamental for reservoir characterization as it detects and groups rocks with similar compositional, petrophysical, and geomechanical qualities. However, challenges exist in performing rock classification in complex carbonate formations that undergo diagenetic overprints. It is common to find disparities between the identified geological facies and petrophysical rock types. This discrepancy may be caused by difficulty in determining the optimum number of rock types and honoring rock fabric in conventional petrophysical rock classification methods. Clustering algorithms, used to perform rock classification, often require the number of clusters as one of the inputs for the algorithm (Halkidi, 2001). Lack of information on this optimum number results in uncertainties in reliable detection of rock types.

Another cause of the disparity between geological facies and petrophysical rock types is the poorly defined relationships between petrophysical properties (i.e., permeability) and geological attributes (i.e., depositional texture) (Skalinski & Kenter, 2013). Poorly defined correlations between petrophysical and geological properties are caused by failure in taking into account rock fabric. Rock fabric affects pore network structure and consequently, the dynamic petrophysical properties of the formation. Quantifying rock fabric will improve rock classification and petrophysical evaluation. This thesis introduces an iterative workflow that simultaneously quantifies rock fabric, improves permeability estimates based on outcomes of rock classification, and optimizes the number of rock classes by minimizing the relative difference in estimates of permeability.

BACKGROUND

Importance of Rock Fabric

Rock fabric refers to spatial distribution of geological attributes that reflect on variable depositional cycles and diagenetic alterations in the formation (Lucia, 2012). Rock fabric has been a significant part of reservoir characterization through identification of depositional texture (Dunham, 1962) and the different pore-space observed in the formation (Choquette & Pray, 1970; Lucia, 1983). From a geological perspective, rock fabric studies are often qualitative descriptions based on core-slabs, thin-section images, Scanning Electron Miscroscope (SEM), and confocal microscopy.

Interparticle porosity, vuggy porosity, and microporosity are the types of complex pore space often found in carbonate formations (Lucia, 1983). Each of these attributes affects petrophysical properties. For instance, vuggy porosity contributes significantly to total porosity. However, isolated vugs do not contribute to fluid flow. In contrast, connected vugs affect the permeability of the formation (Lucia, 1995). These are examples of how rock fabric, as the product of geological processes, considerably affects porosity and permeability of complex formations. Disregarding these complex pore structure may significantly affect the reliablility of petrophysical evaluation and rock classification.

Rock fabric can be quantified using petrophysical parameters that can detect the effect of complex spatial distribution of pore space. One example is by using pore-throat size distribution calculated from Mercury Injection Capillary Pressure (MICP) data. Pore-throat size distribution describes the dynamic petrophysical behavior of the formation in the form of flow capacity and irreducible water saturation (Peters, 2012). Several publications document the application of mathematical functions to model the pore-throat size distribution from MICP data and characterize complex pore systems. Such models

include the Thomeer hyperbolic function (Clerke et al., 2008; Gao et al., 2011) and multi-modal Gaussian function (Xu & Torres-Verdin, 2013; Ferreira et al., 2015; Skalinski & Kenter, 2013). These approaches have been proven beneficial in improving reservoir characterization, petrophysical evaluation, and petrophysical rock classification.

Tortuosity is another parameter used to quantify rock fabric. Rose and Bruce (1949) define tortuosity as the ratio between the effective tortuous path traversed by the electric current and the shortest distance connecting the two ends of the traversed path. Tortuosity is one of the geometrical parameters that controls both fluid and electrical current flow. Kozeny (1927) proposed his heuristically derived permeability model that incorporates tortuosity as one of the geometrical parameters that controls flow capacity of the formation. Berg (2012) also derived an analytical equation for formation factor that incorporates tortuosity, conducting porosity, and constriction factor as parameters that affect electrical properties of the porous media. Herrick and Kennedy (1994) similarly included tortuosity as one of the essential parameters that reduce electric current flow efficiency in porous media. Several publications also document the use of random walk algorithms (Chen & Heidari 2016; Oyewole et al., 2016a) and streamline tracing algorithms (Garcia & Heidari, 2016) in pore-scale numerical simulations to estimate tortuosity of the porous media.

Connected porosity is another example of rock property that needs to be taken into account for reliable rock fabric quantification. Connected porosity is the fraction bulk volume of rock that is occupied by connected pore space and it is typically less than total porosity (Hook, 2003). The difference between connected porosity and total porosity is due to cementation and compaction that reduces the pore space connectivity in the formation. Connected porosity can be estimated from pore-scale image analysis (Garcia & Heidari, 2016; Oyewole et al., 2016a). Hook (2003) stated that compressional-wave-

slowness log can be used to approximate connected porosity. However, this might not be reliable when isolated vugs are present. Compressional-wave-slowness logs measure the velocity of acoustic wave propagation through the rock and does not detect the connectivity of pores. Nonetheless, they can still be used as an approximation for connected porosity and can be improved by incorporating pore-scale image analysis.

Connected porosity includes isolated and stagnant pore-space that does not contribute to fluid flow. Whereas conducting porosity is connected pore space that actively contributes to fluid and electrical current flow (Wempe & Mavko, 2002; Berg, 2012). In complex carbonates, total porosity, connected porosity, and conducting porosity can exhibit significant difference (Wempe & Mavko, 2002; Oyewole et al., 2016a). Combination of pore-scale image analysis and electrical current flow numerical simulation have been used to estimate conducting porosity (Garcia & Heidari, 2016; Oyewole et al., 2016a). Oyewole et al., (2016a) documented an improvement of permeability assessment by incorporating conducting porosity into the pore-scale derived permeability model.

Combining connected porosity, conducting porosity, and tortuosity into a directional connectivity factor is another approach that has been used to quantify rock fabric. Chen and Heidari (2016) proposed a method to calculate directional connectivity of conducting components in porous media by evaluating both tortuosity and volumetric concentration of the conducting components. In this study, the researchers quantified the impact of conducting pyrite and kerogen network in organic-rich mudrocks to improve interpretation of electrical resistivity measurements. Purba et al., (2016) applied the same directional connectivity factor to quantify rock fabric in different rock types of a carbonate formation. In this publication, the directional connectivity factor was found to be consistent in each rock type and therefore can be used as a quantification of rock

fabric. Garcia and Heidari (2016) also performed a combined estimation of directional pore-network connectivity, tortuosity, and constriction factor as rock fabric parameters to improve estimates of water/hydrocarbon saturation. This study documented the use of carbonate pore-scale images as input to numerical simulations of electric current flow to estimate the aforementioned rock fabric parameters.

Incorporating rock fabric into petrophysical evaluation can result in reliable assessment of permeability and water saturation (Wempe & Mavko, 2012; Oyewole et al., 2016a; Purba et al., 2016; Garcia & Heidari, 2016). These improvements further amplify the importance of incorporating rock fabric to improve the reliability of petrophysical evaluation and to enhance reservoir characterization.

Conventional Rock Classification Methods

One of the more geologically driven rock classification methods is Lucia's (1995) method. This classification method has similar principles as Archie's (1952) classification, which focuses on the pore-size distribution and its effect on petrophysical properties. Lucia (1995) classifies two significant rock fabrics, grain-dominated fabric and mud-dominated fabric, based on the mud content and grains or crystals size. This geologically driven method relies heavily on core measurements, (e.g., porosity and permeability), and relates the petrophysical properties to the rock fabric. Other similar geological approaches include the modified Dunham's (1962) classification method by Embry and Klovan (1971) and Choquette and Pray's (1970) generic pore typing. These approaches are simple and directly linked to the depositional environments. However, they are limited to cored zones and it can be challenging to populate the rock classes using well logs in uncored wells (Skalinski & Kenter, 2013). Moreover, number of

classes or facies based on these approaches can be very high and it is challenging to lump them into groups when there is severe diagenetic overprint (Gomes et al., 2008; Mishra et al., 2012; Rebelle, 2014).

Besides geologically driven methods, researchers also use core-based porosity-permeability methods. One example is the Flow Zone Indicator (FZI) method (Amaefule et al., 1993), which clusters core measurements by utilizing the ratio of permeability and effective porosity as representation of flow capacity. However, the FZI method does not incorporate depositional features and may be ineffective when there is no porosity-permeability trend in the core data, often observed in complex carbonates. Moreover, there is also uncertainty in determining the number of rock classes when clustering the core data (Rebelle, 2014).

Carbonate formations can have poor correlation between total porosity and permeability, which cause core-derived methods like the FZI to fail. Therefore, other studies incorporate pore-throat size into the rock classification. Winland's R35 technique (Pittman, 1992) uses Mercury Injection Capillary Pressure (MICP)-based pore-throat radius at 35% as the main attribute to effective flow capacity. This method has been used to group core samples with similar pore-throat size into distinct rock classes (Gunter et al., 2014; Al-Qenae & Al-Thaqafi, 2015). Leverett's J-function (Leverett, 1941) is another method to Winland's R35 which has been widely used for rock classification (Xu et al., 2012; Saneifar et al., 2015). However, these methods fail when core data does not exhibit apparent trends along the iso-pore-throat lines. Uncertainty in number of rock classes in the formation also adds challenges in applying these methods to complex formations.

Clerke et al. (2008) proposed fitting MICP data with Thomeer's (1960) hyperbolic function to represent a single pore system. The Thomeer hyperbolic function

parameters, such as displacement pressure (P_d), bulk volume percentage of mercury at maximum applied pressure (B^{∞}), and pore geometrical factor (G), are used for rock classification. Multimodal pore system requires superposition or a combination of each identified hyperbola function. Another approach is to fit a multi-modal Gaussian distribution to the pore-throat size distribution generated from MICP measurements (Xu & Torres-Verdin, 2013). The fitting parameters from the multi-modal Gaussian distribution are found to be correlated with specific petrophysical properties, such as irreducible water saturation, critical water saturation, and absolute permeability (Xu & Torres-Verdin, 2013; Ferreira et al., 2015). Both Thomeer hyperbola and multi-modal Gaussian functions have similar workflow for rock classification. The fitting parameters of Thomeer hyperbola or multi-modal Gaussian functions from each core sample and number of rock classes are used as inputs to a clustering algorithm (Skalinski and Kenter, 2013). The resulting rock classes are then populated in the log-scale domain using a supervised artificial neural network with core data as the training set (Theologou et al., 2015; Oyewole et al., 2016b). However, limited availability of MICP data from all depth intervals of interest, which may not be readily available.

There have also been publications documenting the use of well logs as inputs for rock classification. Serra and Abbott (1982) introduced Electrofacies as distinct log responses that are linked to a particular rock type and used this principle to perform rock classification. Another approach is to use analytical rock quality factors that relate log responses to dynamic petrophysical properties of the formation (Xu et al., 2012; Gandhi et al., 2010; Heidari et al., 2011; Saneifar et al., 2015). For instance, Xu et al. (2012) evaluate the separation of resistivity logs after mud-filtrate invasion as proxy to pore-size distribution and neutron-density logs cross-over as a proxy to residual hydrocarbon saturation. Alternatively, Saneifar et al. (2015) used separation of resistivity logs for

similar purposes and include volumetric concentration of shale as input to the rock quality factor. These analytical rock quality factors can provide information of the rock fabric that improves rock classification. However, in cases where mud-filtrate invasion effect is not apparent in the resistivity measurements, or there is no obvious cross-over in neutron-density logs, using analytical rock quality factors cannot provide reliable rock classification results.

Previous publications document the impact of reliable petrophysical rock classification towards improvement of permeability assessment and reservoir characterization (Tang, 2008; Skalinski et al., 2009; Moya et al., 2012; Salkia et al., 2016). Conventional petrophysical rock classification methods are able to reliably detect rock types in various cases of carbonate formations. However, these methods have an underlying assumption of prior knowledge of the number of rock classes. This information is challenging to obtain and can considerably affect rock classification results. To the best of this writer's knowledge, this challenge has not been addressed before and is one focus of this thesis. The next subsection of this chapter will discuss the available clustering validation methods that can be used to determine optimum number of rock classes.

Clustering Algorithms and Optimum Number of Rock Classes

As mentioned in the previous subsection, another challenge in performing rock classification is the knowledge of the number of rock classes. Many researchers document the use of K-means clustering, hierarchical clustering, and fuzzy clustering algorithms for rock classification (Tang, 2008; Skalinski & Kenter, 2013; Saneifar et al., 2014; Saneifar et al., 2015). These algorithms often require the number of clusters or

number of rock classes, as one of the inputs (Halkidi et al., 2001). Several techniques address challenges in determining optimum number of clusters. These methods include Monte Carlo cross-validation method (Smyth, 1996), gap statistics method (Tibshirani et al., 2001), and finding the "knee of error" method (Tibshirani et al., 2001; Salvador & Chan, 2004).

The Monte Carlo cross-validation method, introduced by Smyth (1996), involves performing Monte Carlo simulation to determine optimum number of clusters. This method is implemented by defining number of cross-validation runs, changing the number of clusters, and estimating probability density function based on output of the clustering scheme. Then, the defined log-likelihood function is evaluated for each model with different number of clusters to determine the optimum number of clusters. This approach is used to obtain the best fit for the data and avoid overfitting (Sheikholeslami et al., 1998; Salvador & Chan, 2004). However, this approach is computationally expensive.

The Monte Carlo cross-validation method uses the Expectation Maximization (EM) algorithm (Dempster et al., 1977) as the clustering algorithm. There is another approach that combines EM algorithm with Bayesian Information Criterion (BIC) and hierarchical clustering algorithm to determine the best-fit model and optimum number of clusters (Fraley & Raftery, 1998). However, this algorithm cannot be applied to non-Gaussian, high-dimensional, or large datasets (Fraley & Raftery, 2002). This limitation implies that it may not be well-suited for rock classification which requires high-dimensional variables as inputs. Moreover, Bayesian Information Criterion requires prior knowledge of data distribution, which can be challenging to obtain (Weakliem, 1999).

The gap statistics method (Tibshirani et al., 2001) can determine the optimum number of clusters for any given clustering algorithm (e.g., K-Means and hierarchical

algorithm). This method performs the clustering algorithm multiple times with an increasing number of clusters and evaluates weighted distance function of each cluster. As number of clusters increases, weighted distance function will increase in value and reach a maximum point that corresponds to the optimum number of clusters. The gap statistics method has been applied successfully in many clustering problems (Gan et al., 2007; Hastie et al., 2009). Nonetheless, this approach does not perform well under overlapping classes (Fraley & Raftery, 2002; Tibshirani, 2005; Salvador & Chan, 2004).

Another common approach for determining the optimum number of clusters is the "knee of error" method. This method relies on finding the number of clusters corresponding to the point of maximum curvature in the evaluation graph as the optimum number (Salvador & Chan, 2004). Salvador and Chan (2004) stated that the evaluation metric could be computed using distance between clusters, error function, and quality function for all existing data or test-data points. The "knee of error" approach excels compared to the statistical approaches (e.g., Monte Carlo and resampling techniques) since it requires less computational time (Halkidi et al., 2001). This approach can be integrated easily with a hierarchical clustering algorithm used for well log-based rock classification.

PROBLEM STATEMENT

Rock classification of complex carbonate formations is challenging due to the failure to take rock fabric into account in the classification workflow. The rock fabric can be defined as quantified parameters that represent the conducting portion of pore network, connectivity of the pore space, and tortuosity of the pore network. Conventional methods for rock classification that are based on cross-plots of porosity and permeability

fail in capturing rock fabric into rock classification. Other rock classification methods that use MICP data can be used to quantify rock fabric; however, they are limited by availability of data in all depth intervals of interest. Rock classification methods that take advantage of mud-filtrate invasion effects on resistivity logs and separation of neutron-density logs can fail when the aforementioned impacts are not apparent on well logs. Moreover, all of these methods require prior knowledge or assumption of number of rock classes. Determining the optimum number of rock classes is also challenging and has not been addressed in previous publications.

Based on these challenges, using only core or well-log data is not sufficient to quantify rock fabric and incorporate it into rock classification. Pore-scale images, taken from core samples, can provide information about the pore-network geometry and distribution. It can also provide information on conducting pore space and tortuosity of the pore network that can be useful to improve reliability of petrophysical assessment and rock classification. This thesis introduces a new method for improving rock classification by simultaneously quantifying rock fabric, determining the optimum number of rock classes, and improving petrophysical evaluation.

OBJECTIVES

The objective of this thesis is to develop a new method for rock classification in heterogeneous formations that improves petrophysical evaluation by quantifying rock fabric, improving permeability estimates, and determining the optimum number of rock classes.

Detailed list of objectives for this research are as follows:

1. Evaluate pore network connectivity and geometry using a combined evaluation of pore-scale and log-scale measurements in each rock class.
2. Improve rock classification in complex carbonate formations by simultaneously evaluating conducting porosity, permeability, and rock classes in the formation.
3. Determine the optimum number of rock classes in the formation by minimizing a cost function defined by the relative difference of subsequent permeability estimates.

METHOD OVERVIEW

The method proposed in this thesis involves an iterative workflow that starts by assuming one rock class in the entire formation and estimating depth-by-depth permeability using any conventional technique. The number of rock classes is updated by adding a new rock class and an unsupervised neural network is used to perform well log-based rock classification. Hierarchical clustering algorithm (Guha et al., 1998), used in the unsupervised neural network, agglomerates the input data into different sets by minimizing the intra-class variance. Inputs to the neural network are well log-based estimates of petrophysical and compositional properties, including the initial assessment of permeability. Another input is the number of rock classes (i.e., equal to two in the second iteration). Output of this step is the well log-based rock classification, assuming the number of rock classes is equal to two.

Based on classification results from the second iteration, I develop permeability models for each rock class by incorporating pore network geometry features from pore-scale images. Next step consists of updating the depth-by-depth permeability estimates

and calculating the cost function used to optimize number of rock classes. I then increase the number of rock classes by one and repeat the workflow iteratively until the estimates of permeability from two subsequent iterations converge. Outcomes from this iterative workflow are the final rock classification, optimum number of rock classes, and log-scale domain permeability estimates.

THESIS OUTLINE

This thesis consists of four chapters. Chapter 1 describes the motivation for this research and provides background information to rock classification, rock fabric, and determining the optimum number of rock classes. Chapter 2 describes the workflow used to perform rock classification. This section provides a detailed explanation of well-log interpretation, well-log-based rock classification, quantification of rock fabric, pore-scale permeability model development, and determination of the optimum number of rock classes.

Chapter 3 presents the field application of the new workflow in the Scurry Area Canyon Reef Operators Committee (SACROC) unit. This chapter describes the application of the method used for rock classification and quantification of rock fabric. The presented results are optimum number of rock classes, final rock classification, and permeability estimates in log-scale domain. For comparison purposes, conventional porosity-permeability method is used to estimate permeability in log-scale domain. Permeability estimates from the proposed and a conventional method are then compared by calculating the average relative error between permeability estimates and core permeability measurements. Discussion of the application of the introduced method to the

field data will follow the results. Chapter 4 presents the summary and conclusion of this thesis, recommendation for best practices, and future work.

Chapter 2: Method[1]

This chapter describes methods used to improve rock classification and petrophysical evaluation by optimizing the number of rock classes and integrating rock fabric into rock classification. The first subsection discusses the cost function used to determine optimum number of rock classes. The next subsection explains pore-scale numerical simulations performed to generate permeability models for each rock class. The final subsection discusses the connectivity factor defined in pore-scale domain as a quantification of rock fabric and for validating the rock classification results.

ITERATIVE WORKFLOW FOR DETERMINING OPTIMUM NUMBER OF ROCK CLASSES

Cost Function Development

Cost function is used as the evaluation metric to determine optimum number of rock classes. "Knee of error" method is used to optimize the number of rock classes. This method evaluates increasing or decreasing trend of the cost function as number of classes changes; the "knee of error" is the point at which significant local change in value of cost function occurs (Halkidi et.al., 2001). This point in the cost function versus number of classes plot indicates clusters that are homogeneous and dissimilar to each other (Salvador & Chan, 2004).

In applying this method for rock classification, the cost function includes a parameter that is directly affected by rock fabric. In carbonate reservoirs with complex

---

[1] Purba, S. A., Garcia, A. P., & Heidari, Z. (2017, June). New Method for Rock Classification in Carbonate Formations Using Well-Log-Based Rock Fabric Quantification. In SPWLA 58th Annual Logging Symposium. Society of Petrophysicists and Well-Log Analysts. This thesis writer contribution is introduction and application of the new workflow.

pore network geometry, the rock fabric discerns one rock type from another and. In this thesis, rock fabric is incorporated by using log-scale permeability estimates as inputs to the cost function. The rock fabric is represented in the pore-scale derived permeability models used to perform the log-scale domain permeability assessment.

The proposed method involves an iterative procedure that improves well-log-based rock classification and permeability assessment as I update the number of rock classes to minimize a cost function, $C(i, k^{(i)}_{est,n})$. The cost function is defined as

$$C(i,k^{(i)}{}_{est}) = \frac{100}{N}\sum_{n=1}^{N}\left|\frac{\log(k^{(i+1)}{}_{est,\mathrm{n}} - k^{(i)}{}_{est,\mathrm{n}})}{\log(k^{(i+1)}{}_{est,\mathrm{n}})}\right|, \tag{2.1}$$

where $k^{(i)}_{est,n}$ is the estimated well-log-based permeability (mD) corresponding to i number of rock classes, N is the total number of available data points (i.e., the number of data points in the estimated permeability logs), and n is the index associated with a given data point. The objective is to find the optimum number of rock classes by minimizing the relative difference in permeability estimates in two subsequent iterations. This can be achieved in the absence of core permeability measurements.

If core permeability measurements are available, I define an alternative cost function as the average relative error in permeability estimates via

$$C(i,k^{(i)}{}_{est,n}) = \frac{100}{N}\sum_{n=1}^{N}\left|\frac{\log(k^{(i)}{}_{est,\mathrm{n}} - k^{(i)}{}_{\mathrm{core,n}})}{\log(k^{(i)}{}_{\mathrm{core,n}})}\right|, \tag{2.2}$$

where $k^{(i)}_{core,n}$ is the actual permeability (mD) from core measurements and N is the total number of available data points (i.e., the number of core samples in this case). Estimated permeability, used to evaluate the alternative cost function, is taken from the same depth in which core data is available.

Both cost functions, when evaluated in the same formation, should result in the same trend and optimum number of rock classes. As number of rock classes increases, value of the cost function should decrease until it reaches point of convergence. Number of rock classes corresponding to the convergence point is the optimum number of rock classes. In other words, refining the rock classes past this optimum point no longer improve permeability estimates.

Application of the Proposed Rock Classification Workflow

Figure 2.1 shows the overall workflow in applying the cost function to determine optimum number of rock classes. The introduced workflow begins with the assumption of having one rock class in the formation and proceeds to well-log interpretation. Joint interpretation of conventional well logs is used for preliminary assessment of volumetric concentrations of minerals, water saturation, fluid-corrected resistivity, and acoustic porosity. Inputs to the multi-mineral analysis include gamma ray (GR), neutron porosity, bulk density, compressional-wave-slowness, photoelectric factor (PEF), and resistivity logs. Acoustic porosity is calculated using Wyllie's time-average equation (Wyllie at al., 1956) using compressional-wave slowness log as input. Acoustic porosity is used as an approximation to the connected porosity. Connected porosity is used as input into the pore-scale derived permeability models.

Archie's equation is used to calculate water saturation. Archie's parameters used for water saturation assessment are assumed to be 1, 2, and 2, for Archie's Winsauer factor (Winsauer et al., 1952), a, Archie's porosity exponent, m, and Archie's saturation exponent, n, respectively. Fluid-corrected deep resistivity (Rdeep_FC) is calculated using Archie's equation as an approximation to the fully water-saturated formation resistivity.

The inputs to calculate Rdeep_FC are water saturation estimates, deep resistivity log, and the Archie's saturation exponent, n. Fluid-corrected deep resistivity is also used as input into the pore-scale derived permeability model. The next subsections will describe the pore-scale derived permeability model. This model is used to estimate permeability in log-scale domain for the second and next iterations. For the first iteration, however, conventional core porosity-permeability correlation is used to obtain depth-by-depth permeability estimates.

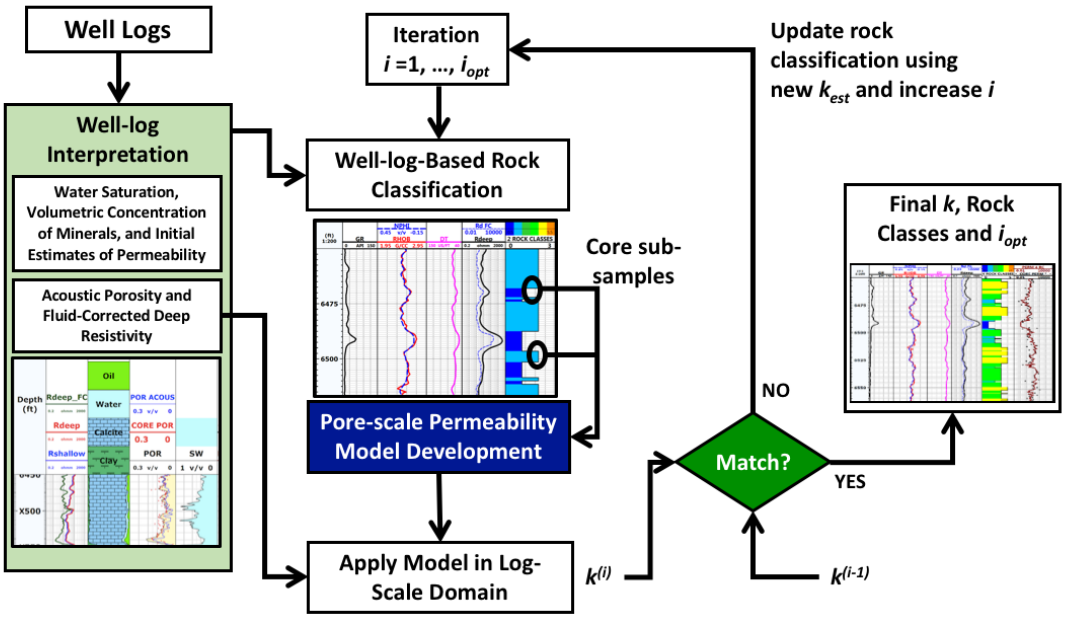

Figure 2.1: Workflow describing the iterative method to improve rock classification and permeability assessment by determining the optimum number of rock classes.

The number of rock classes is updated by adding a new rock class and an unsupervised neural network is used to perform well-log-based rock classification. Inputs to the unsupervised neural network are the well-log-based estimates of petrophysical and compositional properties. Another input is the number of rock classes (i.e., equal to two

in this second iteration). A hierarchical clustering algorithm (Guha et al., 1998) is used to agglomerate the input data into different sets by minimizing the intra-class variance. Output of this step is the depth-by-depth rock class for two rock classes.

Based on the classification results from the second iteration, I develop permeability models for each rock class by incorporating pore network geometry features. Permeability model development performed in pore-scale domain will be discussed in the next subsection. Next step consists of updating the depth-by-depth permeability estimates and calculating the cost function using Equation (2.1). Number of rock classes is then increased by one and the workflow is repeated iteratively until the estimated cost function converges to its minimum value. Outcomes of this iterative workflow are the final rock classification, optimum number of rock classes, and depth-by-depth permeability estimates.

PERMEABILITY MODEL DEVELOPMENT

Permeability model development workflow used in this thesis is based on the workflow introduced by Oyewole et.al. (2016a). Figure 2.2 shows the workflow for developing the permeability model for each rock class. The first step includes acquiring three-dimensional (3D) pore-scale images from core samples taken in each rock class in the formation. The 3D volumes of the rock sample are then processed to convert them into stacks of 2D gray-scale images. These gray-scale images are binarized and used as inputs for pore-scale numerical simulations. Electric current and fluid flow numerical simulations will result in spatial distribution of electric potential and pressure in porous media, respectively. Estimated spatial distribution of electric potential and pressure are used to estimate conducting porosity and permeability, respectively. Permeability models

for each rock class are developed by obtaining correlation between permeability and conducting porosity of the pore-scale rock images. The following subsections will discuss in more detail the acquisition of pore-scale images and methods used for numerical simulations.

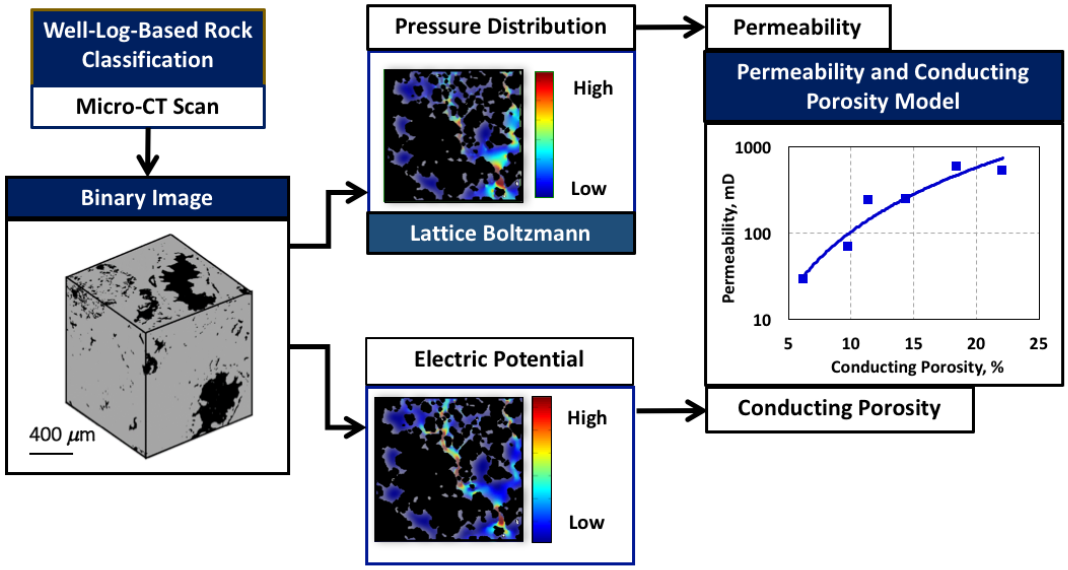

Figure 2.2: Workflow describing pore-scale permeability model development as proposed by Oyewole et al. (2016a).

Three-dimensional (3D) Pore-Scale Imaging and Image Segmentation

Based on the initial rock classification results, I obtained pore-scale samples from four-inch diameter whole core samples that were cut into three-to-five millimeter cubes. I obtained high-resolution 3D pore-scale images of the rock samples at different depths using a Micro-Computed Tomography (CT) imaging equipment. Micro-CT equipment uses high energy X-ray generated from the source to penetrate the rock sample from different angles as the rock sample is rotated. Micro-CT scanner obtains the two-

dimensional (2D) absorption profile of the rotating rock sample. The 2D absorption profile is used to reconstruct 3D volume of the rock, which consists of a stack of 2D gray-scale images.

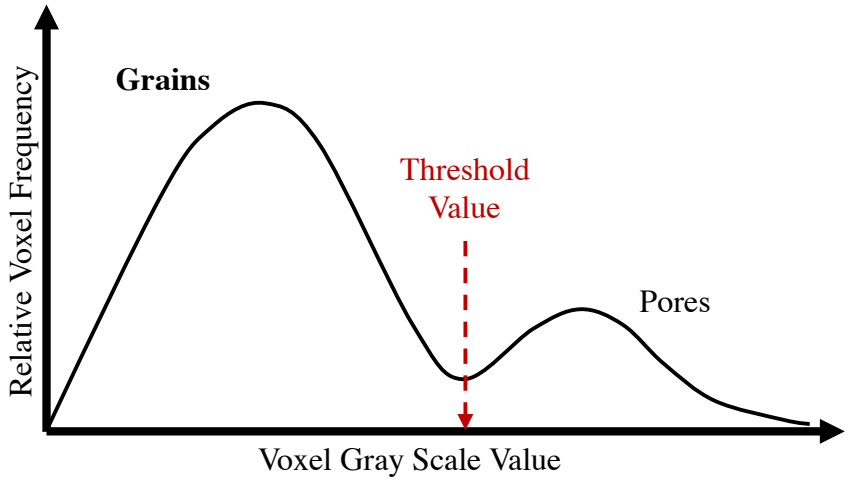

Figure 2.3: Example of a voxel gray-scale histogram. The first peak in the gray-scale histogram corresponds to the high-intensity pixels representing the grains. The second peak corresponds to the low-intensity pixels representing the pores.

Fiji ImageJ (Schindelin et al., 2012), an open-source image processing software, is used to perform image segmentation to convert the stack of 2D gray-scale rock images into binary images. *Threshold* software feature is used to segment each image pixel based on its intensity. Figure 2.3 shows an example of a voxel intensity histogram. The first peak in the histogram corresponds to high-intensity pixels representing the grains. The second peak in the histogram corresponds to low-intensity pixels representing the pores. Based on the gray-scale intensity histogram, the gray-scale threshold can be selected at the transition between pores and grains. The *Threshold* feature will then segment pixels

with intensity values higher than the threshold value from pixels with intensity values lower than the threshold value.

In addition, *3D Trainable Weka Segmentation* feature in the Fiji ImageJ software is used to improve segmentation when resulting binary images from the *Threshold* feature does not satisfy visual inspection. Figure 2.4 shows an example of a binarized gray-scale image. Black and white regions represent pores and grains, respectively.

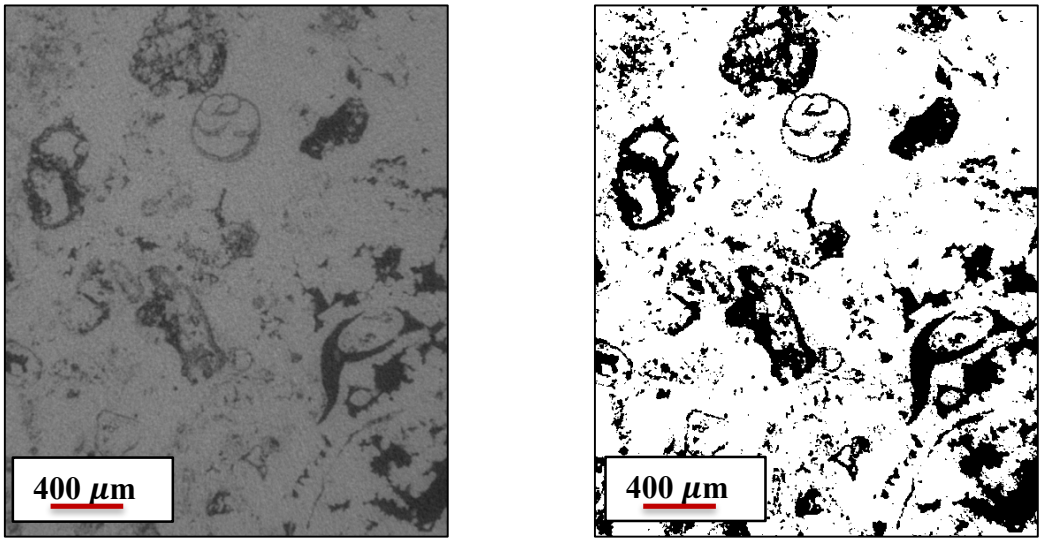

(a) (b)

Figure 2.4: (a) Gray-scale micro-CT image. (b) Segmented image. Pores and grains are represented as black and white pixels, respectively.

Electrical Current Flow Simulation

Electrical resistivity of the pore-scale rock samples is used to estimate conducting porosity of the pore network. Electrical resistivity of the 3D pore-scale images is calculated by simultaneously solving Ohm's Law defined as

$$J = -\sigma \nabla \Phi \,, \tag{2.3}$$

together with Kirchoff's Current Law for steady-state electrical conductivity, given by

$$\nabla \cdot J = \nabla \cdot \left(\sigma \nabla \Phi \right) = 0, \tag{2.4}$$

with constant electric potential in opposing faces of the image. J is the electrical current density (A/m^2), σ is the electrical conductivity, and Φ is the electric potential (V/m). Pore-scale rock images are assumed to be fully saturated with brine with conductivity (σ) equivalent to electrical conductivity of formation water. Brine is assumed to be the only conductive element in the formation. Electrical conductivity of the grains is assumed to be zero.

Electrical resistance of the fully water-saturated pore-scale rock samples, R, is calculated via

$$R = \frac{\Delta \Phi}{\int J dA}, \tag{2.5}$$

where A is the cross-sectional area (m^2) of the 3D pore-scale image.

Electrical current flow simulation is necessary to obtain the electrical resistivity of the 3D pore-scale images. Process of the numerical simulation starts by generating tetrahedral mesh of the voxelized 3D pore-scale rock images by using Delaunay triangulation (Fang & Boas, 2009). Elmer, an open-source Multiphysics solver, is used to solve for total current and electric potential of the pore network. Inputs to the solver are tetrahedral mesh of the 3D pore-scale images and electric potential difference in the pore-scale images. Outputs of the solver are electrical current density and electric potential used as inputs to calculate electrical resistivity of the fully water-saturated pore-scale rock images (Equation 2.5).

Assessment of Tortuosity and Conducting Porosity

Tortuosity is used alongside the formation factor of the pore-scale rock images to calculate conducting porosity. Tortuosity of the porous media is estimated using a streamline tracing algorithm. This algorithm is based on the semi-analytical particle tracking method developed by Pollock (1988) but adapted for electrical conductivity problem (Garcia & Heidari, 2016). First step is to obtain electric current densities calculated from the electrical current flow simulation results. Electric current density is assumed to vary linearly in each direction of the voxels based on net electric current density change in the corresponding direction inside each voxel (Garcia & Heidari, 2016). Electric current density in the x-direction is proportional to drift velocity of the electrical charges, expressed as

$$\rho \frac{dx}{dt} = J_{i,j,k} + (J_{i+1,j,k} - J_{i,j,k}) \frac{x}{\Delta x}, \tag{2.6}$$

where the electric current densities $J_{i,j,k}$ and $J_{i+1,j,k}$ are current densities entering and leaving the voxel in the x-direction, Δx is the length of the voxel in the x-direction, and ρ is the electric charge density (charge per unit volume). Electrical charge density is assumed to be constant since brine is assumed to be the only conductive element in the porous media. Solving Equation (2.6) results in the travel time of the electric charge to travel through the length of voxel in the x-direction. Then, time of flight is estimated as the sum of all travel times for an electric charge to move across the rock sample from high potential to low potential voxel. The estimated time of flight is then used to calculate electrical tortuosity of the 3D pore-scale rock images.

Electrical tortuosity, τ_e, is calculated by the weighted average of each streamline by the inverse of time of flight (Zhang & Knackstedt, 1995), given by

$$\tau_e = \frac{1}{L} \frac{\sum_{i=1}^{n_{sl}} \frac{L_{ei}}{TOF_i}}{\sum_{i=1}^{n_{sl}} \frac{1}{TOF_i}}, \tag{2.7}$$

where n_{sl} is the total number of streamlines, L_{ei} is the length of each streamline, and TOF_i is the time of flight associated with each streamline.

Connected porosity is estimated using a two-way travel 3D Connected-Component Labeling (CCL) algorithm to identify connected porosity of the pore-scale binary images (Garcia & Heidari, 2016). This algorithm detects the fraction of pore network that connects opposing faces of the 3D pore-scale image. Input to this algorithm is the 3D pore-scale binary images and the output is connected porosity of the porous media. Connected porosity is different than the conducting porosity because it includes dead-end pores that do not contribute to electric current and fluid flow.

Conducting porosity of the pore-scale rock images is then estimated using resistivity of fully water-saturated rock, water resistivity, and tortuosity of the pore system (Wyllie & Rose, 1950) via

$$\phi_e = \frac{\tau_e}{F}, \tag{2.8}$$

where F is the formation factor, τ_e is the electrical tortuosity, and ϕ_e is the conducting porosity. Conducting porosity represents the effective porosity that contributes to fluid and electrical current flow. Therefore, this parameter quantifies rock fabric as the volume fraction of conducting pore space in the formation.

Performing this procedure in log-scale domain requires depth-by-depth estimates of tortuosity. Therefore, I also defined a model that links electrical tortuosity to connected porosity via

$$\tau_e = c\phi_c^{\,d}, \tag{2.9}$$

where τ_e is the electrical tortuosity, ϕ_c is the conducting porosity, c, and d are the calibration parameters. This tortuosity model is used in log-scale domain for estimating depth-by-depth electrical tortuosity. Connected porosity in the log-scale-domain is approximated by the estimates of acoustic porosity that are used as inputs to the tortuosity model. Both depth-by-depth estimates of tortuosity and formation factor, obtained from the resistivity logs, are then used as inputs to Equation 2.8 to estimate depth-by-depth conducting porosity.

Fluid Flow Simulation

To obtain permeability of the pore-scale rock images, Lattice Boltzmann Method (LBM) is used to perform numerical simulations of fluid flow. Lattice Boltzmann Method is a discrete computational fluid dynamic method that simulates Newtonian fluid flow by discretizing Boltzmann transport equation on a lattice mesh. This method has been widely applied for simulating fluid flow in porous media (Chen & Doolen, 1998; Chi & Heidari, 2014; Oyewole, 2016a; Garcia & Heidari, 2016).

Palabos, an open-source LBM solver (Palabos, 2013), is used to simulate single-phase fluid flow in the pore-scale rock images. Brine is assumed to be the fluid in the porous media. Pore-scale binary images, predetermined pressure gradient, fluid viscosity, and dimensions of the voxelized images are used as inputs to the solver. Output of the solver is the average velocity within the pore network.

Permeability Assessment and Model Development

Using average velocity obtained from the fluid flow simulation, permeability of the pore-scale rock images, k, is calculated via Darcy's law, given by

$$U = -\frac{k}{\mu}\frac{p_{inlet} - p_{outlet}}{h}, \tag{2.10}$$

where U is the fluid velocity in m/s, μ is the dynamic viscosity of the fluid in Pa.s, p_{inlet} is the inlet pressure in Pa, p_{outlet} is the outlet pressure in Pa, and h is the height of the voxelized segmented image in m.

Permeability models for each rock class are developed using the LBM permeability and estimated conducting porosity, defined as

$$k = a\phi_e^{\,b}, \tag{2.11}$$

where a and b are the calibration parameters specific for each rock class. Rock fabric is incorporated in the permeability model by using estimates of conducting porosity. The developed permeability models are applied in the log-scale domain to estimate depth-by-depth permeability at each iteration using depth-by-depth estimates of conducting porosity.

Log-scale-domain estimates of permeability calculated using the pore-scale derived permeability models are used as inputs to the rock classification algorithm. As number of rock classes increases, the rock classes are updated and several pore-scale rock images are repopulated into new rock classes. Permeability models for these updated rock classes can be generated using the estimated parameters (i.e., conducting porosity, connected porosity, permeability, resistivity, and tortuosity). In the case of rock classes without pore-scale rock images, conventional core-based porosity-permeability correlation is used instead of the pore-scale permeability model.

ASSESSMENT OF CONNECTIVITY FACTOR FOR ROCK FABRIC QUANTIFICATION

Connectivity factor used in this thesis is based on the work done in Purba et al. (2016), which was an adaptation from Chen and Heidari (2016). Previous publication by Chen and Heidari (2015) evaluates the connected network of electrically conducting components in rocks by defining a directional connectivity factor (Ψ) along *i*-direction (x, y, or z) via

$$\Psi_i = \sum_{j=i}^{M} \frac{Z_j}{\beta \tau_{j,i}^{\gamma}}, \tag{2.12}$$

where j is the order index for the connected clusters of the conductive component, M is the total number of connected conductive clusters along i-direction, Z_j is the volumetric concentration of the j^{th} connected conductive cluster, β and γ are connectivity parameters, and $\tau_{j,i}$ is the directional tortuosity of the j^{th} connected cluster of each conductive component along i-direction. Chen and Heidari (2016) applied this connectivity factor in pore-scale domain to evaluate the effect of spatial distribution of conductive kerogen and pyrite on electrical conductivity of organic-rich mudrocks.

In this thesis, the connectivity factor is used to quantify the spatial distribution of connected pore network. Similar definition of the connectivity factor presented by Chen and Heidari (2016) is applied to the case where saline water is the only conducting phase in the porous media. Therefore, Equation 2.10 reduces to

$$\Psi = \frac{1}{\beta} \frac{\phi_c}{\tau_e^{\gamma}}, \tag{2.13}$$

where β and γ are the connectivity parameters, ϕ_c is the connected porosity, and τ_e is the tortuosity of the porous media. Electrical tortuosity and connected porosity estimates are

used as inputs to quantify the connectivity factor. The connectivity factor defined above is a geometrical parameter that represents pore network structure, which affects both fluid flow and electric current flow. This parameter can quantify rock fabric and remain consistent in the same rock class. In this thesis, this connectivity factor is used to cross-validate the final rock classification results.

Chapter 3: Field Application: SACROC Unit[2]

This chapter presents an application of the proposed method described in Chapter 2 to the SACROC Unit.

INTRODUCTION TO SACROC UNIT

The Scurry Area Canyon Reef Operators Committee (SACROC) Unit is the largest producing unit in the Greater Horseshoe Atoll of the Permian Basin of West Texas with 2.8 billion stock tank barrels (STB) of original oil-in-place (OOIP). Figure 3.1 shows the location of the Horseshoe Atoll, which is in the eastern half of the Midland Basin, the eastern sub-basin of the overall Permian Basin of western Texas and southeastern New Mexico (Isdiken, 2013).

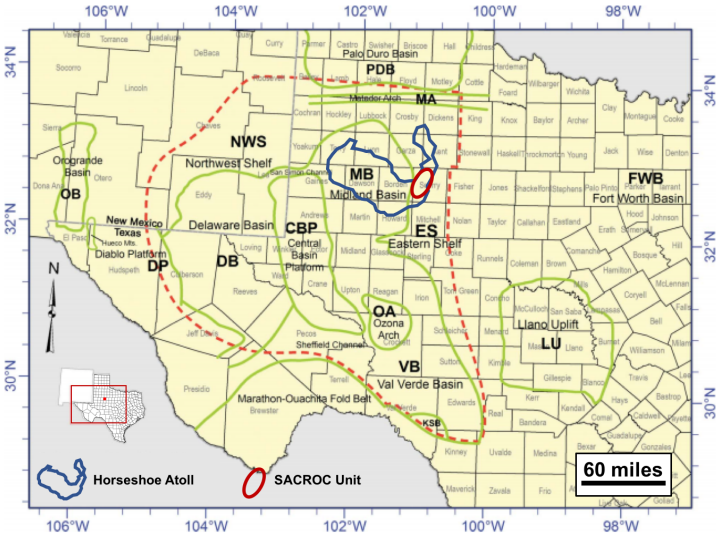

Figure 3.1: The Horseshoe Atoll and SACROC Unit location map within the Permian Basin (red dashed line) and its surrounding area in West Texas (Modified from Wright, 2011).

[2] Purba, S. A., Garcia, A. P., & Heidari, Z. (2017, June). New Method for Rock Classification in Carbonate Formations Using Well-Log-Based Rock Fabric Quantification. In SPWLA 58th Annual Logging Symposium. Society of Petrophysicists and Well-Log Analysts. This thesis writer contribution is introduction and application of the new workflow.

SACROC Unit is a Pennsylvanian-aged carbonate platform reservoir deposited during the peak icehouse system. Main producing formations are the Canyon and Cisco Formations, each with its own distinct depositional and diagenetic attributes. Tectonic activity, icehouse settings, post-burial geochemical processes, and complex depositional system are considered the main causes of the heterogeneity. Karstification, moldic porosity, touching vuggy porosity, and fractures are examples of the geologic attributes affiliated with both Canyon and Cisco Formations.

SACROC unit can be divided into three geographic regions based on its productive portion, Northern Platform, Central Plain, and Southwestern Region (Raines, 2003). Southwestern Region has the lowest net pay and complex structure (Reeves, 2007). Central Plain has a broad, gently arching plain, broken by steep-sided pinnacles, gentle mounds, intermittent sinuous lows, and localized depressions. Central Plain area is the current focus of CO_2 flood projects in SACROC unit. Northern Platform area has the thickest overall interval and is also characterized with complex geometry and compartmentalization (Reeves, 2007). Wolfcamp shale, overlaying the Cisco and Canyon Formations, constitute the top and lateral seal for the reservoir and is believed to be the source for the hydrocarbon in the reservoir (Gonzales et al., 2008).

Canyon Formation is described to have thin layers of cyclic open-shelf subtidal carbonate cycles with minimal diagenetic overprint through Early and Middle Canyon deposition and followed by high energy shoal cycles and sequence scale erosion during the Late Canyon (Isdiken, 2013). Cisco Formation is described to have pinnacle reef and complex fractured muddy crinoid-dominated facies with vuggy porosity (Kerans, 2001). Cisco Formation is also characterized by non-layered intervals on the platform and clinoformal layers at the wedges. Both Canyon and Cisco Formations are mostly composed of limestone and a minor amount of shale beds (Isdiken, 2013).

RESULTS AND DISCUSSION

Application of the Iterative Rock Classification Workflow to SACROC Unit

I performed joint interpretation of the conventional well-logs for two wells drilled in the SACROC unit. Tables 3.1 and 3.2 list the parameters assumed in the well-log interpretation of Well No. 1 and Well No. 2.

Parameters	Values	Unit
Formation water resistivity @86º F	0.04	ohmm
Formation water salt concentration	190,000	ppm
Mud-filtrate resistivity @86º F	0.21	ohmm
Mud-filtrate salt concentration	25,500	ppm
Shale porosity	0.1	-

Table 3.1: SACROC Unit Field Example, Well No. 1: Assumed input parameters for well-log interpretation.

Parameters	Values	Unit
Formation water resistivity @86º F	0.04	ohmm
Formation water salt concentration	190,000	ppm
Mud-filtrate resistivity @86º F	0.34	ohmm
Mud-filtrate salt concentration	15,000	ppm
Shale porosity	0.08	-

Table 3.2: SACROC Unit Field Example, Well No. 2: Assumed input parameters for well-log interpretation.

Main lithology in both wells is limestone with minor amount of shale. Therefore, calcite and shale are the assumed input for multi-mineral analysis. Compressional-wave-slowness of grains and fluid are assumed to be 47.6 μs/ft and 189.1 μs/ft, respectively. Density of grains and fluid are assumed to be 2.71 g/cm^3 and 1 g/cm^3, respectively. Formation fluids include saline formation water and oil. The drilling mud is saline water-based mud. Archie's equation is used to calculate water saturation. Archie's parameters used for water saturation assessment are assumed to be 1, 2, and 2, for a, m, and n, respectively.

Inputs to the multi-mineral analysis are the gamma ray (GR), electrical resistivity, density, neutron porosity, photoelectric factor (PEF), and compressional-wave-slowness logs. Figure 3.2 shows the outcomes of the well-log interpretation that includes volumetric concentrations of minerals, depth-by-depth estimates of acoustic porosity, and water saturation. Acoustic porosity is used as a preliminary estimate of connected porosity, calculated using the compressional-wave slowness log (Wyllie et al., 1956). I corrected deep resistivity for the effect of initial fluids in the formation by fluid substitution using Archie's equation. The fluid substitution process requires deep resistivity, estimates of porosity, Archie's Winsauer factor, a, and Archie's porosity exponent, m, as inputs. Then, I used conventional core porosity-permeability correlation to obtain depth-by-depth permeability estimates for the first iteration.

After the first iteration, I proceeded to increase the number of rock classes and use an unsupervised artificial neural network to perform the well-log-based rock classification. The unsupervised neural network uses Hierarchical clustering algorithm (Guha et al., 1998). Well-logs interpretation results (i.e., acoustic porosity, volumetric concentrations of minerals, fluid-corrected resistivity estimates, and permeability estimates from the previous iteration) and number of rock classes are inputs to the

artificial neural network algorithm used to detect the rock classes. Based on the results of this classification, pore-scale rock samples from different depths are obtained and used to develop the permeability models.

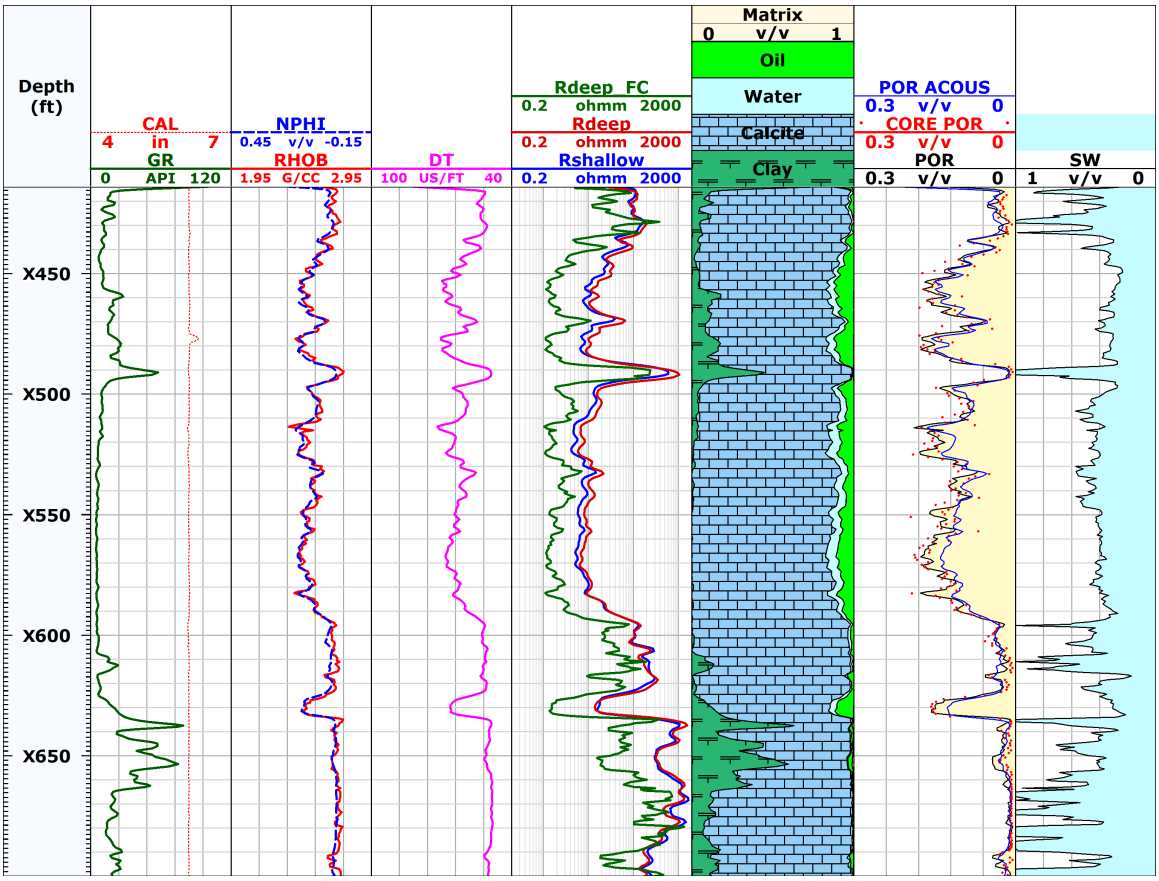

Figure 3.2: SACROC Unit, Well No. 1: Conventional well logs and well-log interpretation results. Track 1: depth; Track 2-5: caliper, gamma-ray (GR), neutron porosity in limestone units, bulk density, compressional slowness, fluid-corrected deep resistivity, deep resistivity, and shallow resistivity logs; Track 6: volumetric concentration of minerals and fluids; Track 7-8: estimated acoustic porosity, core porosity data, estimated total porosity, and estimated water saturation.

After each iteration of the workflow, the updated permeability estimates are used as an additional input to the classification algorithm method for updating the well-log-

based rock classification. Since the rock classification and number of rock classes vary in each iteration, the available core subsamples are re-populated based on the updated rock classes, and the permeability models are updated. This iterative process is repeated until optimum number of rock classes and convergence in the permeability estimates are achieved. Equation 2.1 is used for optimizing the number of rock classes without incorporating core permeability measurements, to demonstrate the performance of the iterative workflow in the absence of core measurements. Core measurements are then used for cross-validating the permeability estimates. The next subsection discusses the development of permeability models in the pore-scale domain.

Development of Permeability Models in the Pore-Scale Domain

Scanning, processing, and binarizing rock samples are performed by members of our research group (Oyewole et al., 2016a; Purba et al., 2016) and me. We obtain 3D pore-scale binarized rock images with a resolution of 2-3 μm/pixel. The binary images are converted into binary digital matrices to be used as inputs for pore-scale numerical simulation of fluid flow and electric current flow. Figure 3.3 illustrates examples of the binarized pore-scale images that are used in this thesis (for Rock Type 1 to 4). The micro-CT scanner resolution is not high enough to detect pore-throat radii in pore-scale images, from Rock Type 1. Since the pore throats are not detected, outcomes of the pore-scale numerical simulations of fluid and electrical current flow in this rock type can be inaccurate. Permeability may be underestimated and resistivity may be overestimated, which leads to uncertainty in the depth-by-depth permeability assessment. Therefore, the proposed workflow for permeability model development could not be applied to this rock type. In such cases, conventional permeability assessment technique is used instead. The

proposed workflow for permeability model development is only applied to pore-scale samples with large enough pore-throat size detected in the resulting binary images (i.e., Rock Types 2, 3, and 4) from the micro-CT imaging method.

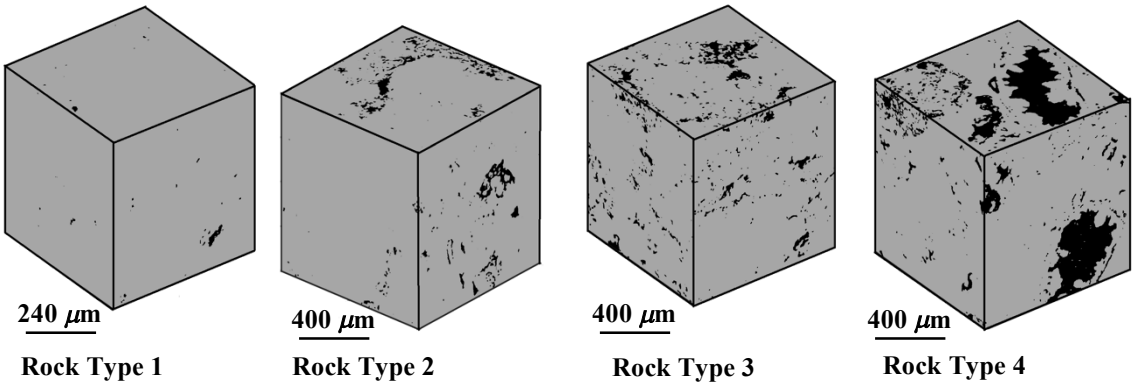

Figure 3.3: Pore-scale binary rock images obtained from Rock Classes 1 to 4 . Black and gray regions represent pores and grains, respectively.

Elmer, a multiphysics solver, is used to perform pore-scale electrical current simulation to calculate electrical resistivity (Oyewole et al., 2016a). Palabos, an open-source LBM solver (Palabos, 2013), is used to perform pore-scale single-phase fluid flow simulation (Oyewole et al., 2016a). Streamline tracing algorithm, developed in the research group, is used to evaluate tortuosity (Garcia & Heidari, 2016). CCL algorithm, developed in the research group (Garcia & Heidari, 2016), is used to estimate connected porosity of the pore-scale rock images. I obtained a power-law correlation between tortuosity and connected porosity to derive the tortuosity model for each rock class. Figure 3.4 illustrates tortuosity model as a function of connected porosity for the final rock classes that is applied in log-scale domain. In this example, connected porosity is approximated by acoustic porosity, estimated from compressional-wave-slowness log. Estimates of connected porosity are used as input to the tortuosity model in each rock class to estimate depth-by-depth tortuosity in log-scale domain. Depth-by-depth

tortuosity and fluid-corrected resistivity estimates from the well-log interpretation results are inputs to Equation 2.8 for determining the conducting porosity in log-scale domain.

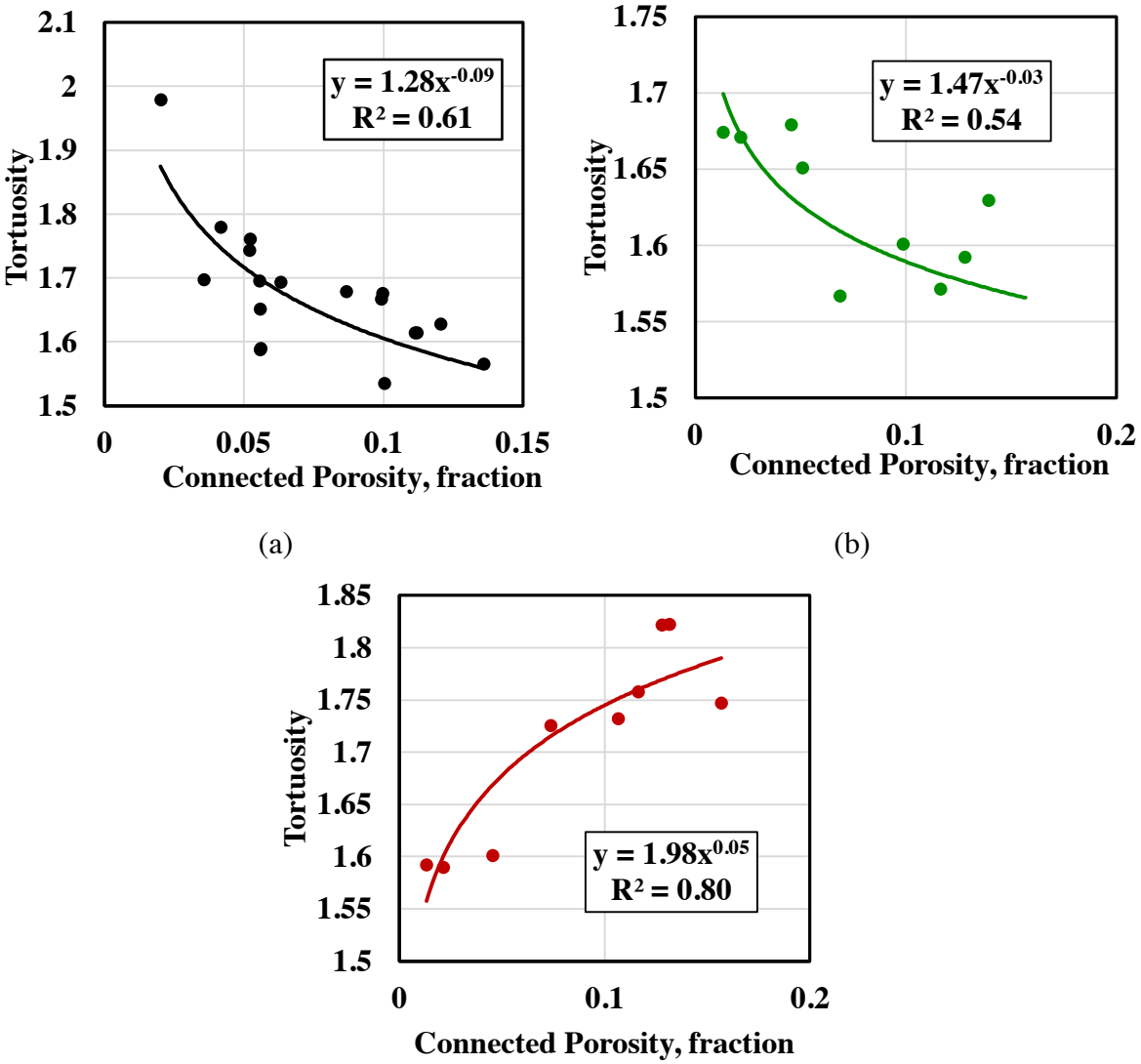

Figure 3.4: Pore-scale correlation between connected porosity and tortuosity in (a) Rock Type 2, (b) Rock Type 3, and (c) Rock Type 4.

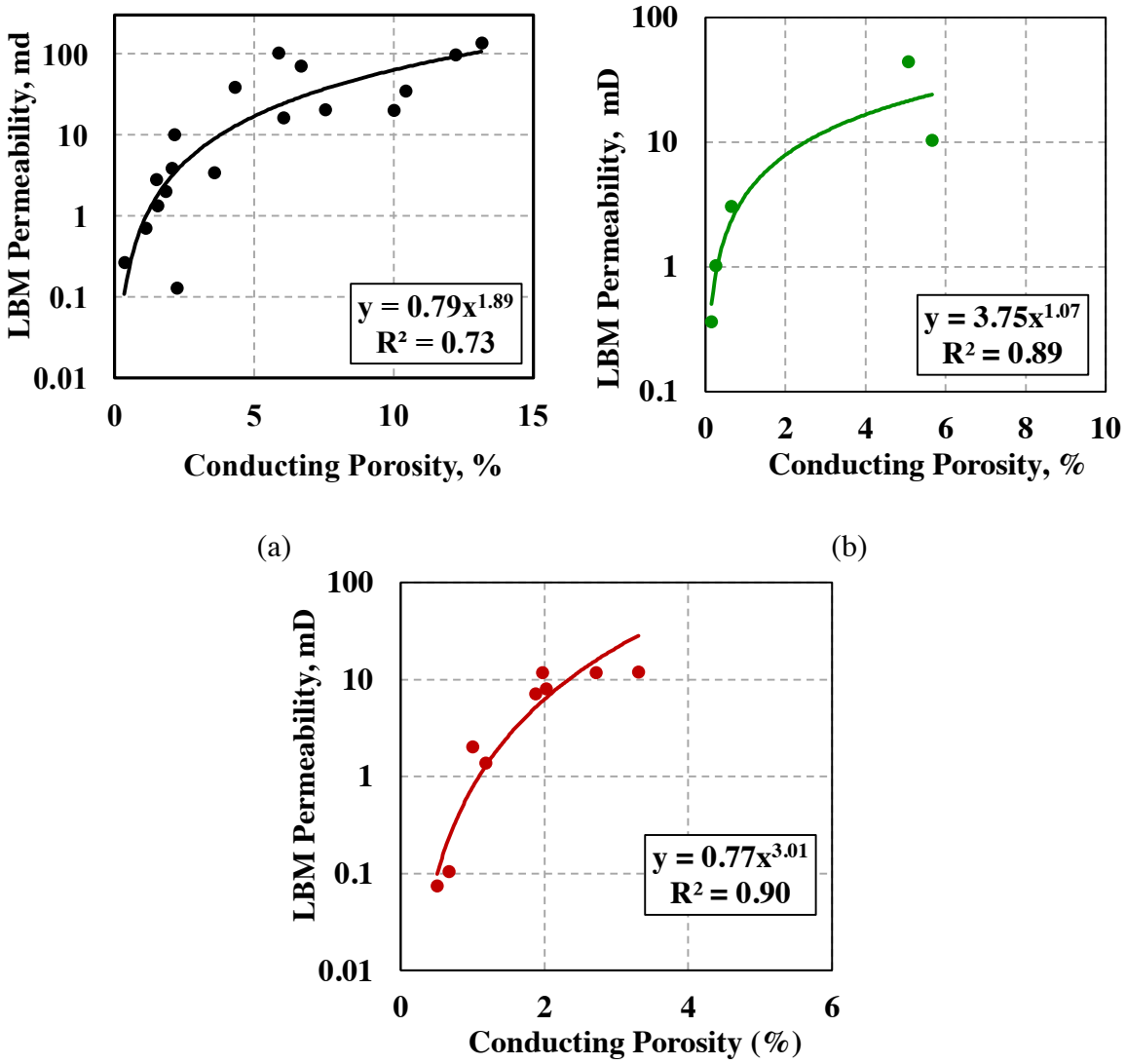

Figure 3.5: Pore-scale correlation between permeability and conducting porosity in (a) Rock Type 2, (b) Rock Type 3, and (c) Rock Type 4.

Permeability model is developed based on relationship found between permeability estimates and conducting porosity estimated from pore-scale numerical simulations of fluid flow (LBM) and electric current flux, respectively, for each rock

class. Figure 3.5 illustrates the relationship between conducting porosity and simulated LBM permeability in the final rock classes. These permeability models are used for permeability assessment in log-scale domain. Depth-by-depth estimates of conducting porosity from Equation 2.8 are inputs to these permeability models.

Optimizing the Number of Rock Classes

The optimum number of rock classes is obtained by minimizing the introduced cost function (Equation 2.1). Figure 3.6 shows value of the cost function calculated at each iteration for Well No. 1. Number of iterations is equivalent to number of rock classes in this thesis. In Well No. 1, the cost function value at the first iteration is very high, at approximately 200%. As I iterate through the proposed workflow, value of the cost function decreases as number of rock classes increases. This decrease implies that increasing the number of rock classes reduces average relative difference between two subsequent iterations of permeability estimates. In Well No. 1, value of the cost function remains below 10% after four iterations. This convergence after four iterations indicates additional rock classes will not result in significant improvement in the permeability estimates. Thus, the optimum number of rock classes in Well No.1 is equal to four.

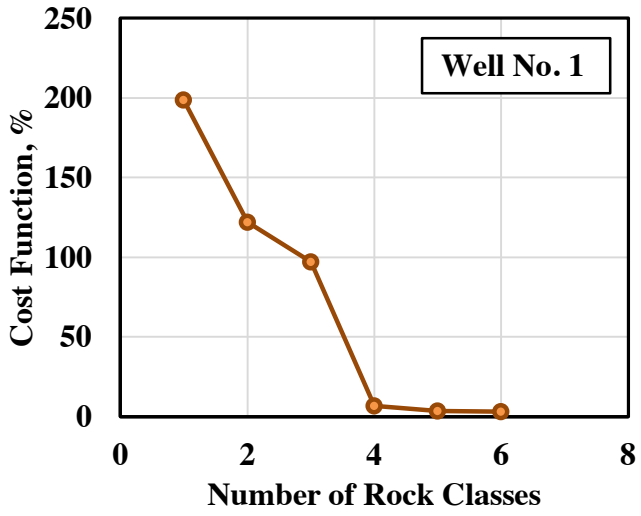

Figure 3.6: SACROC Unit, Well No. 1: Calculated cost function (Equation 2.1) plotted as a function of the number of rock classes (i.e., equivalent to the number of iterations).

Figure 3.7 shows value of the cost function at each iteration for Well No. 2. Initial value of the cost function at the first iteration is also very high, at approximately 180%. As number of rock classes increases, the cost function value decreases until it converges after four iterations. Therefore, optimum number of rock classes in Well No. 2 is four. The optimum number of classes obtained in both wells is in agreement. The cost function produces consistent results in both wells and can result in the same optimum number of rock classes in other wells in this formation.

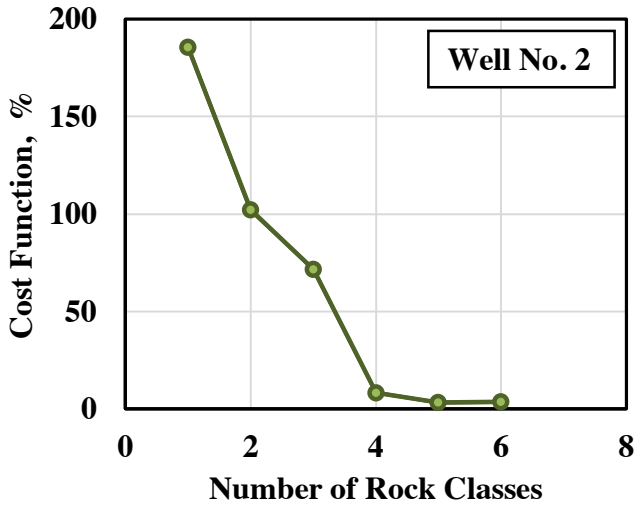

Figure 3.7: SACROC Unit, Well No. 2: The calculated cost function (Equation 2.1) plotted as a function of the number of rock classes (i.e., equivalent to the number of iterations).

Furthermore, to verify the reliability of the iterative workflow, I calculate the average relative difference between the permeability estimates and the core measurements using Equation 2.2. Figures 3.8 and 3.9 show the average relative error in permeability estimates as a function of number of rock classes for Well No. 1 and Well No. 2, respectively. The results demonstrate a significant drop of 95% and 137% in relative errors in permeability estimates in Well No. 1 and Well No. 2, respectively. This consistent trend observed in both wells displays the impact of increasing the number of rock classes on improving permeability estimates. The calculated average relative difference asymptotes to a value of 48%, and 45%, for Well No. 1 and Well No. 2, respectively, after four iterations. The average relative difference does not decrease significantly after four iterations and therefore indicates that the optimum number of rock classes is four.

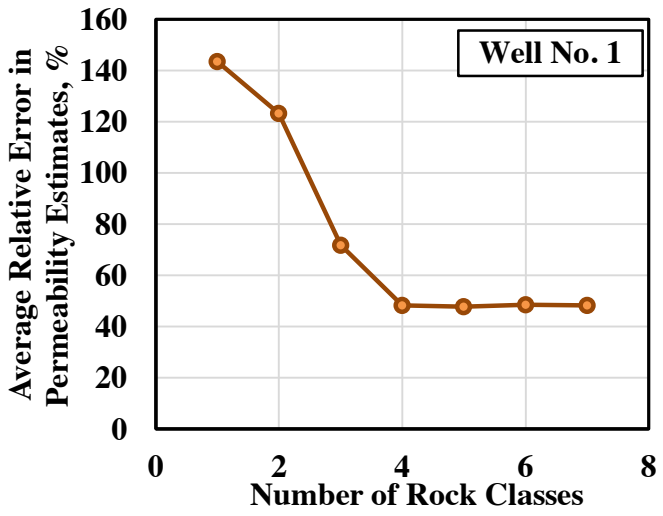

Figure 3.8: SACROC Unit, Well No. 1: Average relative error in permeability estimates plotted as a function of the number of rock classes (i.e., equivalent to the number of iterations in this case.

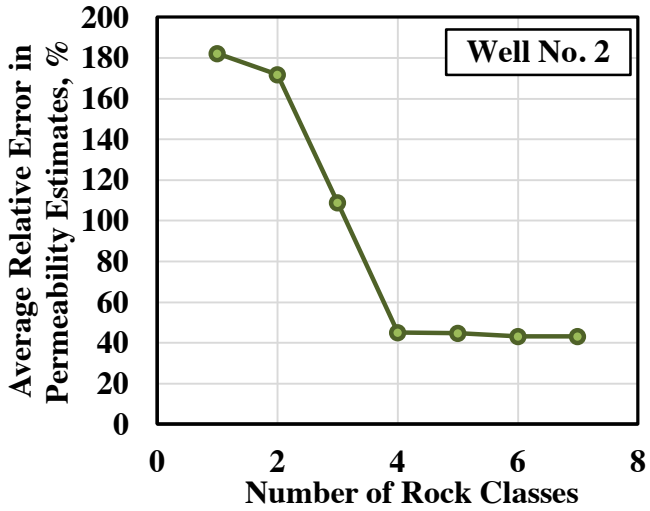

Figure 3.9: SACROC Unit, Well No. 2: Average relative error in permeability estimates plotted as a function of the number of rock classes (i.e., equivalent to the number of iterations in this case.

Cost function defined by Equation 2.2 does not converge to zero, unlike the cost function defined by Equation 2.1. A possible reason behind this trend is the difference in

measurement resolution of pore-scale rock images and well logs. Geologic features such as vugs and fractures can be detected by well logs used for permeability assessment. These features, however, may not be detected in pore-scale rock images used for permeability model development and in core measurements. This limitation introduces uncertainty in evaluating conducting porosity in log-scale domain and consequently, in log-scale permeability assessment. This will affect the convergence in the cost function defined by Equation 2.2.

Another significant point from the results displayed in Figures 3.6 to 3.9 is both cost functions (Equations 2.1 and 2.2) result in the same optimum number of rock classes. This consistency indicates that the cost function can be used for optimizing number of rock classes in wells without core measurements.. In this field example, however, there are rock types with pore-throats that could not be detected in the pore-scale rock images. In these rock types, conducting porosity cannot be reliably estimated and can add uncertainty to the estimates of permeability and consequently, to the optimum number of rock classes.

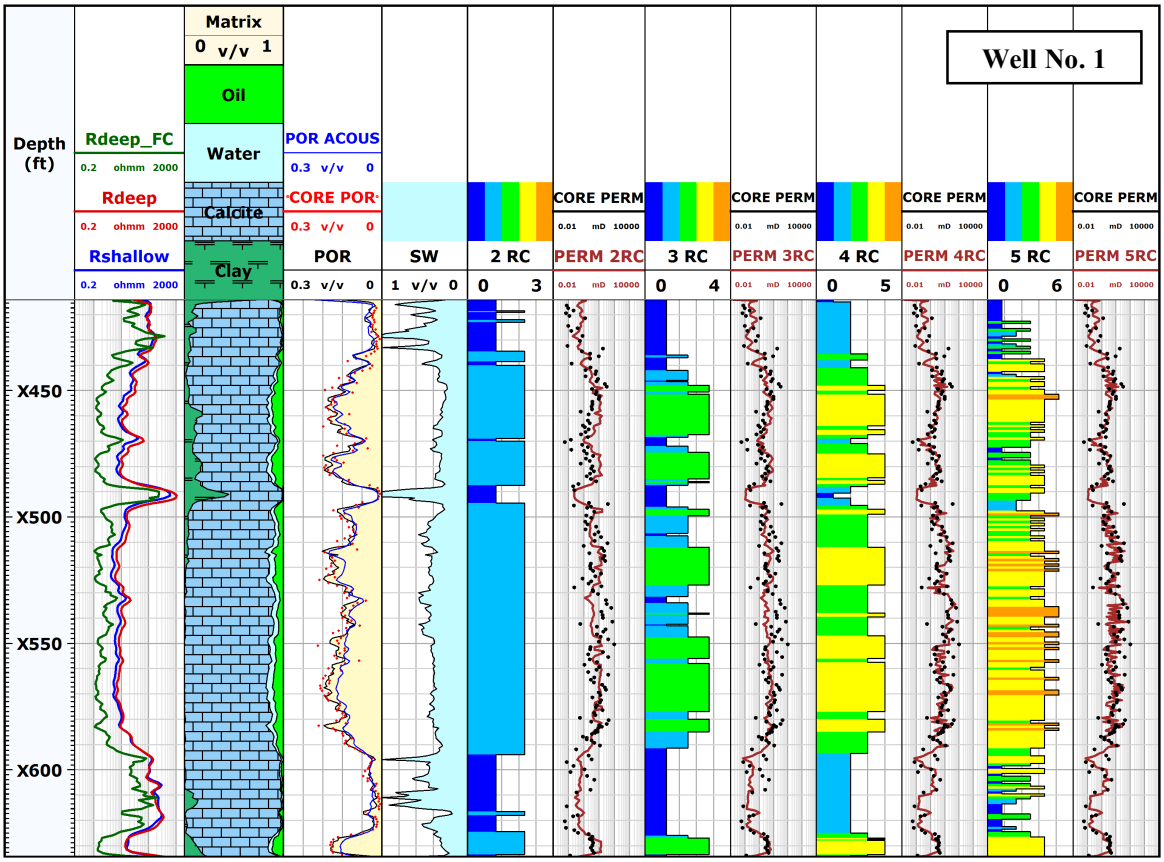

Figure 3.10: SACROC Unit, Well No. 1: Comparison of the rock classification results at number of rock classes ranging from 2 to 5. Track 1: depth; Track 2: fluid-corrected deep resistivity, deep resistivity, and shallow resistivity; Track 3-5: estimated volumetric concentration of minerals and fluid, acoustic porosity, total porosity, water saturation, and core porosity measurements; Track 6-13: rock classification results and estimated permeability at each iteration, and core permeability measurements.

Final Rock Classification Results and Improvement in Permeability Estimates

Figure 3.10 shows results of the rock classification and permeability assessment for number of rock classes ranging from 2 to 5, in Well No. 1. As number of rock classes increases, the permeability estimates converge to the core measurements. As previously stated, the optimum number of rock classes is four. Figures 3.11(a) and 3.11(b) compare estimates of permeability using conventional core-based porosity-permeability

correlations and the introduced method against core measurements, respectively, at the optimum number of rock classes (i.e., four rock classes) in Well No. 1. I observe a 62% improvement of permeability estimates in all rock classes using the proposed method compared to those obtained from conventional method.

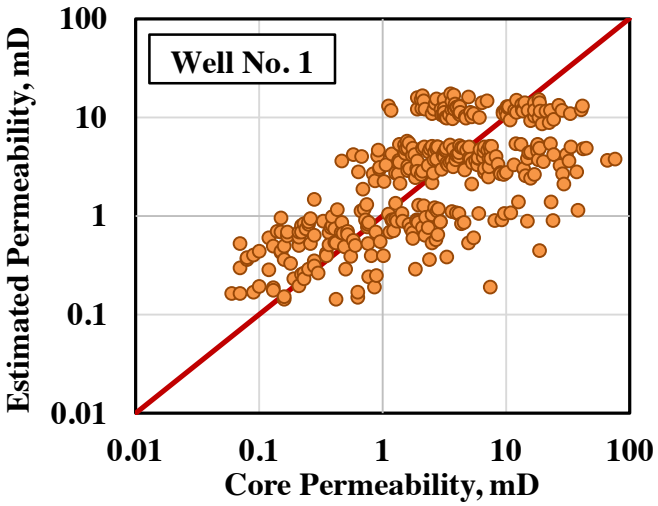

(a)

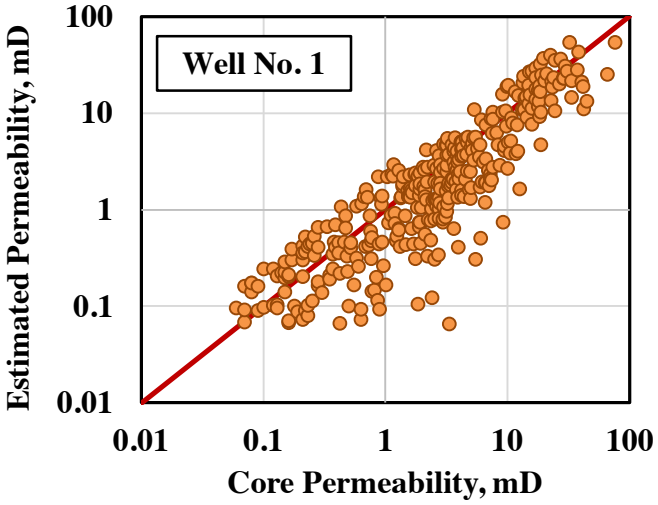

(b)

Figure 3.11: SACROC Unit, Well No. 1: Comparison of estimates of permeability using (a) conventional method against core measurements and (b) the introduced method against core measurements.

Figure 3.12 shows results of the rock classification and permeability assessments for number of rock classes ranging from 2 to 5, in Well No. 2. As number of rock classes increases, permeability estimates converge to the core measurements, the same trend observed in Well No. 1. These two similar trends further indicate the consistency of the proposed method in optimizing the number of rock classes.

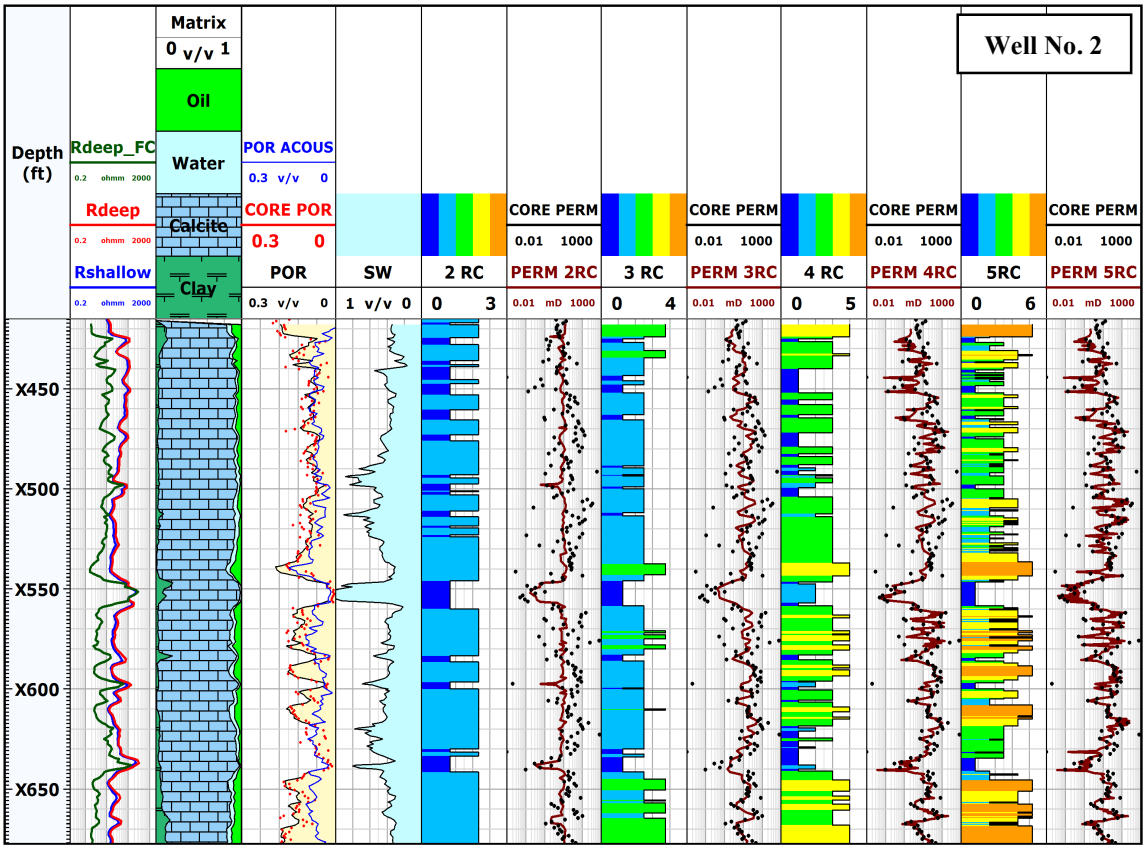

Figure 3.12: SACROC Unit, Well No. 2: Comparison of the rock classification results at the number of rock classes ranging from 2 to 5. Track 1: depth; Track 2: fluid-corrected deep resistivity, deep resistivity, and shallow resistivity; Track 3-5: estimated volumetric concentration of minerals and fluid, acoustic porosity, total porosity, water saturation estimates, and core porosity measurements; Track 6-13: rock classification results and estimated permeability at each iteration, and core permeability measurement.

Figures 3.13(a) and 3.13(b) compare estimates of permeability using conventional and introduced methods against core measurements, respectively, in Well No. 2.

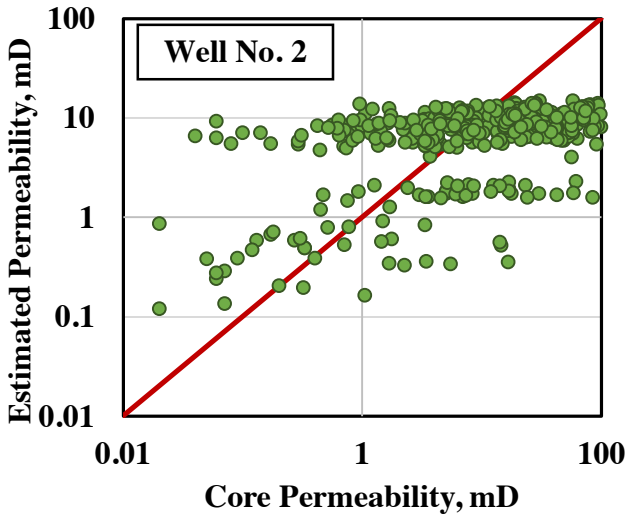

(a)

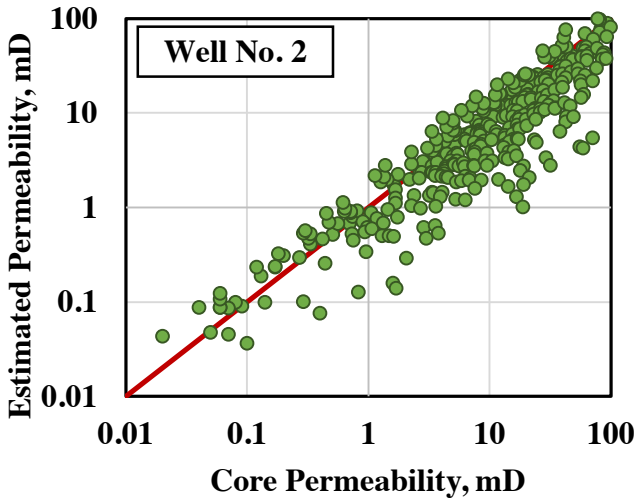

(b)

Figure 3.13: SACROC Unit, Well No. 2: Comparison of estimates of permeability using (a) the conventional method against core measurements and (b) the introduced method against core measurements.

I observe a 75% improvement in permeability estimates using the proposed method compared to those obtained from conventional core-based porosity-permeability correlation in Well No. 2.

Results show that the introduced workflow improved permeability estimates by up to 75% compared to an adopted conventional method based on porosity-permeability correlations. Results confirm importance of quantifying rock fabric in each rock type in the formation and populating it in log-scale domain for well-log-based permeability assessment and rock classification. Furthermore, number of rock classes affects reliability of permeability assessment and an optimized number of rock classes can significantly improve formation evaluation. However, populating it in log-scale domain requires an underlying assumption that acoustic porosity estimated from the compressional-wave-slowness log is a reliable estimate for connected porosity. Moreover, Archie's equation is assumed to be applicable for estimating the fluid-corrected resistivity. In cases where formation's wettability is altered, in presence of complex pore structure, or when clay minerals are present, using Archie's equation can result in unreliable fluid-corrected resistivity estimates. Failure to fulfill these two assumptions can lead to higher uncertainty in performing log-scale permeability assessments using the proposed workflow. In such cases, use of conventional well-log-based permeability assessment in each rock class is recommended.

Comparison Against Identified Depositional Facies

After obtaining optimum number of rock classes, the final rock classification results are compared against the identified depositional facies. Depositional facies are obtained from the available literature (Wright, 2011; Isdiken, 2013). Table 3.2 lists all

identified depositional facies in Well No. 2. There is a wide range of facies with mud-dominated and grain-dominated fabric among the listed identified depositional facies. This wide range of rock fabric is typical in an icehouse carbonate platform system. High-amplitude, high-frequency sea level changes contribute to this complexity (Read & Horbury, 1993).

Formation	Depositional Facies	Rock Class
Canyon	Crinoidal Wackestone	1
	Mud-dominated Packstone	2
	Fossil Grain-dominated Packstone	3
	Crinoid-fusulinid Grain-dominated Packstone	
	Ooida Grain-dominated Packstone	4
	Debris Flow	
Cisco	Crinoidal Wackestone	1
	Crinoidal Mud-dominated Packstone	2
	Mud-dominated Packstone	
	Crinoid-fusulinid Grain-dominated Packstone	3
	Sponge-algal Boundstone	
	Moldic Grainstone	4
	Debris Flow	

Table 3.2: SACROC Unit, Well No.2: List of identified depositional facies, obtained from Wright (2011) and Isdiken (2013) and their respective equivalent rock types in both Canyon and Cisco Formations.

Previous publications document 13 identified depositional facies in SACROC unit (Wright, 2011; Isdiken, 2013). In order to make an equal comparison between these identified geological facies and the final petrophysical rock classes, several facies are lumped based on Lucia's (1995) classification method. As shown in Table 3.2, number of rock classes for lumping the depositional facies is kept as four to be consistent with optimum number of rock classes obtained from the proposed technique.

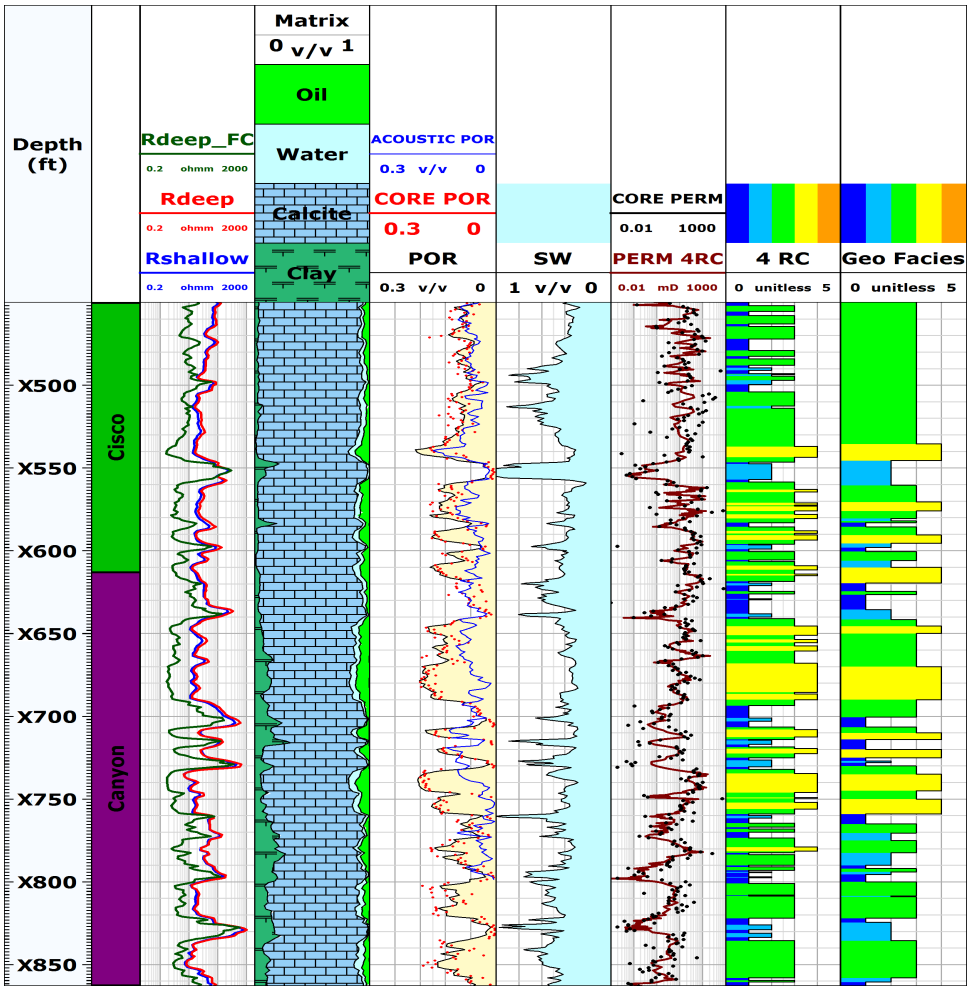

Figure 3.14: SACROC Unit, Well No. 2: Comparison of the final rock classification results against the identified geological facies. Track 1-2: depth and formation zones. Track 3-4: shallow resistivity, deep resistivity, fluid-corrected deep resistivity, and volumetric concentration of minerals. Track 5-6: total porosity estimates, acoustic porosity estimates, core porosity, and water saturation estimates. Track 7: final permeability estimates and core permeability. Track 8-9: final rock classification result and identified depositional facies.

Figure 3.14 compares the identified petrophysical rock classes against the depositional facies. Both rock classes and geological facies are in agreement, indicating that the proposed workflow is able to incorporate rock fabric quantitatively. For instance,

Rock Class 1 has the lowest reservoir quality and is associated with wackestone facies. Wackestone has the highest mud content and smallest grain size compared to other depositional facies (Isdiken, 2013). In Figure 3.13, depth intervals associated with the wackestone facies (Rock Class 1) have the lowest porosity and permeability values. This indicates a poor-quality reservoir, since having low porosity and permeability implies low productivity zone or even flow barrier. High mud-content facies are also correlated with smaller pore-throat size and microporosity (Isdkien, 2013). This micropores result in limited detection of the pores in the pore-scale binary images used for deriving the permeability models. This causes uncertainty in the permeability assessment and rock classification results. Facies with grain-dominated, grain-dominated packstone and the grainstone, correlates well with Rock Classes 3 and 4. Rock Classes 3 and 4 both exhibit good rock quality, which corresponds to higher porosity and permeability values.

There are several depth intervals in Cisco Formation where there is discrepancy between petrophysical rock classes and depositional facies, specifically with the sponge-algal boundstone facies. In Dunham's (1962) classification scheme, boundstone is a carbonate rock where the original components are bound together during deposition. This facies correlates to coarse skeletal grains deposited with significantly fine carbonate grains and mud resulting in a complex pore network structure. This poor sorting fabric often found in boundstone facies constitutes a large range of permeability values. The proposed workflow detects this complexity by clustering the boundstone interval into two rock classes instead of one. Moreover, extensive diagenetic overprint, such as karstification and vuggy porosity, commonly found in Cisco Formation can amplify this difference in the identified rock classes.

Cross-validation using Estimated Pore-scale Connectivity Factor

I calculated the probability density function of estimated pore-scale connectivity factor for the four identified rock classes. Figure 3.14 illustrates the probability density function in Rock Classes 2, 3, and 4.

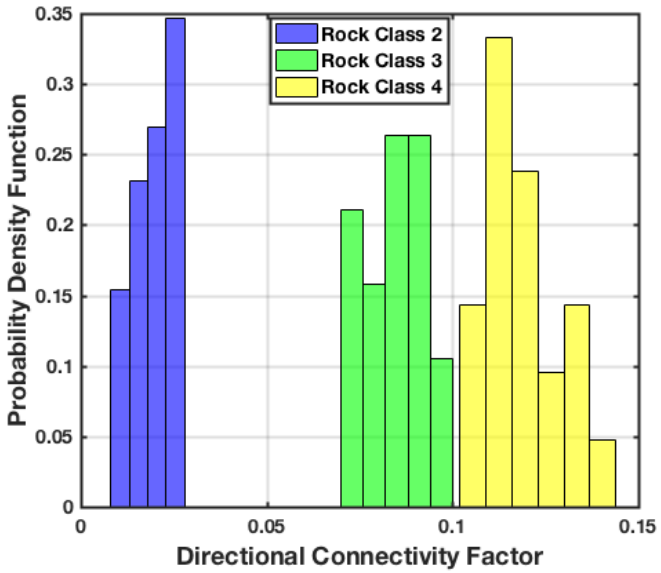

Figure 3.15: Probability density function of estimated connectivity factor in three out of four different rock classes. Connectivity factor is estimated from the pore-scale images of the rock samples collected at different depth intervals.

Results shown in Figure 3.14 indicate that the estimated connectivity factor remained consistent in each rock class. Moreover, Rock Class 4 has the highest average value of connectivity factor, which corresponds to high reservoir quality of this rock class. The defined connectivity factor captures the complexity of pore network structure in the rock and therefore can be used to cross-validate rock classification results. It should be noted, however, that assimilating rock fabric in the proposed workflow requires high-resolution images to quantify pore network geometry. In this field example, Rock Class 1 has the poorest reservoir quality among all four rock classes. Rock Class 1 has

tight pore throats that could not be captured by the micro-CT scanner. Thus, connectivity factor could not be estimated for Rock Class 1 because the pore throats are smaller than the resolution of the micro-CT scanner. Furthermore, as stated in the second subsection of this chapter, uncertainty on the outcomes of the introduced method increases, if pore throats are smaller than the resolution of the imaging technique.

Chapter 4: Summary and Conclusions

This chapter reiterates my conclusions and summarizes the main contribution of the research conducted in this thesis. Provided are recommendations for best practices and future research.

SUMMARY

The objective of this thesis was to develop a rock classification method that simultaneously quantifies rock fabric, optimizes the number of rock classes, and improves petrophysical evaluation and rock classification. I successfully applied the proposed iterative workflow of well-log-based rock classification in two wells in a carbonate formation. Here are the main contributions of the research described in this thesis compared to conventional techniques:

- Introduced an iterative rock classification method that simultaneously determines the optimum number of rock classes, quantifies rock fabric, and improves petrophysical evaluation. The proposed method integrates pore- and log-scale formation data and interpretation techniques.
- Determined the optimum number of rock classes by minimizing a cost function, defined as the average relative difference in permeability estimates in two subsequent iterations. The proposed cost function can be applied in wells without core permeability measurements.
- Applied the introduced method successfully to two wells drilled in the SACROC unit.

- The cost function defined in Equation 2.1 showed convergence after four iterations. The cost function value at the first iteration reached up to 200% and decreased significantly to below 10% at after four iterations in both wells.
- The cost function defined in Equation 2.2 also converged after four iterations. The cost function converged to 48% and 45% in Well No.1 and Well. No 2, respectively.
- Both cost functions defined in Equations 2.1 and 2.2 resulted in the same optimum number of rock classes. In the field case applied for this thesis, optimum number of rock classes was consistently estimated to be four.
- Quantified rock fabric using the connectivity factor and used it to cross-validate results of rock classification and optimum number of rock classes. The connectivity factor reflected quality of the rocks and was consistent in each rock class. In the field case applied for this thesis, Rock Class 4 has the best quality and Rock Class 1 has the lowest quality.
- Rock classification results from the proposed workflow detected similar trend in rock classes based on the reservoir quality when compared to the identified depositional facies.
- The rock classification workflow allowed improvement of formation evaluation, shown by the decrease of average relative error of permeability estimates and core permeability measurements when compared against conventional core porosity-permeability correlation method. I observed 62% and 75% decrease of relative error in Well No. 1 and Well No. 2, respectively.

CONCLUSIONS

This subsection lists the conclusions drawn from the results presented in this thesis.

1. The proposed method enables determination of optimum number of rock classes using well logs with minimal core-based calibration efforts.
2. The number of rock classes in both wells was found to be in agreement. Moreover, both cost function definitions (Equations 2.1 and 2.2) resulted in the same optimum number of rock classes.
3. The rock classification results agreed with the identified depositional facies. This accordance indicates that the proposed iterative workflow was able to integrate the relationship between rock fabric and petrophysical properties into the rock classification.
4. The proposed rock classification workflow improves the reliability of the permeability assessment by up to 75% when compared against conventional porosity-permeability correlations. This confirmed the importance of quantifying rock fabric in each rock type in the formation and populating it in log-scale domain for well-log-based permeability assessment and rock classification.
5. The calculated connectivity factor remains consistent in each rock type and can be used to cross-validate the rock classification results. However, the quantitative connectivity factor requires high-resolution pore-scale rock images to identify pore throats.

RECOMMENDATIONS FOR BEST PRACTICES

The proposed rock classification method in this thesis simultaneously determines the optimum number of rock classes, quantifies rock fabric, and improves formation

evaluation. The following list describes the recommendations for best practices in petrophysical rock classification:

1. Determining the optimum number of rock classes have significant impacts on improving rock classification and formation evaluation. Therefore, it is recommended for formations with complex pore structure and composition.
2. Rock-fabric-dependent parameters, such as permeability, can be used as inputs to the cost function used to optimize number of rock classes. This approach will simultaneously improve rock classification and petrophysical evaluation in complex and heterogeneous formations.
3. In the absence of core permeability measurements, the cost function in Equation 2.1 should be used to determine the optimum number of rock classes. If core permeability measurements are available, the cost function in Equation 2.2 can be used instead of Equation 2.1.
4. Pore-scale images can be used as inputs to quantify pore network structure and connectivity. This approach is recommended for improving permeability assessment and cross-validating rock classification results in complex formations.
5. Quantitatively incorporating rock fabric information into well-log-based rock classification results in rock classes that capture the rock quality and are consistent with identified geological facies. This approach is recommended to enhance reservoir characterization in complex formations.
6. In quantifying rock fabric using 3D pore-scale images, it is recommended to obtain pore-scale rock images from each rock type in the formation.

RECOMMENDATIONS FOR FUTURE WORK

This thesis focused on addressing some of the challenges often found in performing rock classification in complex carbonate formations. Those challenges include optimum number of rock classes, poorly defined relationships between geologic and petrophysical interpretations, as well as reliability of petrophysical properties assessment. However, there remain many unsolved problems that have not been addressed in this thesis. The following list describes possible research ideas for future work that could expand the contribution of this thesis:

1. Automation of the proposed workflow.
2. Expansion of the proposed cost function by including other rock-fabric-dependent petrophysical properties.
3. Introduction of new upscaling techniques for reliable extrapolation of petrophysical properties from fine measurement scale to log and field scales in complex formations.
4. Integrating core slab images or image logs into the proposed workflow to allow detection of vugs in the formation.

List of Symbols

β	:	Connectivity parameter
γ	:	Connectivity parameter
μ	:	Fluid viscosity, [Pa.s]
Ψ	:	Connected factor
σ	:	Electrical conductivity, [s/m]
ϕ_c	:	Connected porosity, [fr.]
ϕ_e	:	Conducting/effective porosity, [fr.]
τ_e	:	Electrical tortuosity
Δ	:	Length of the voxel in the x-direction, [m]
A	:	Cross-sectional area, [m^2]
a	:	Calibration parameter
b	:	Calibration parameter
B^{∞}	:	Bulk volume percentage of mercury at maximum applied pressure
c	:	Calibration parameter
C	:	Cost function at i rock classes, [%]
d	:	Calibration parameter
F	:	Formation factor
G	:	Pore geometrical factor
h	:	Sample height, [m]
i	:	Number of rock classes
J	:	Electrical current density, [A/m^2]
$J_{i,j,k}$	:	Electric current density entering voxel i, j, k, [A/m^2]
$J_{i+1,j,k}$	:	Electric current density exiting voxel i, j, k, [A/m^2]

k : Permeability, [mD]

$k^{(i)}_{core,n}$: Core permeability, [mD]

$k^{(i)}_{est,n}$: Estimated permeability at i number of rock classes, [mD]

L_{ei} : Length of each electrical streamline, [m]

n : Index of point

N : Total data points

N' : Total data points

P_d : Displacement pressure

p_{inlet} : Inlet pressure, [Pa]

p_{outlet} : Outlet pressure, [Pa]

R : Resistivity of fully-water saturated rock, [ohm.m]

R_{deep_FC} : Fluid-corrected deep resistivity, [ohm.m]

TOF_i : Time-of-flight, [s]

U : Fluid velocity, [m/s]

ρ : Electric charge density, [A.s/m^3]

Φ : Electric potential, [V]

List of Acronyms

2D	:	Two-Dimensional
3D	:	Three-Dimensional
BIC	:	Bayesian Information Criterion
CCL	:	Connected Component Labeling
CT	:	Computed Tomography
FZI	:	Flow Zone Indicator
GR	:	Gamma-Ray
LBM	:	Lattice-Boltzmann Method
MICP	:	Mercury Injection Capillary Pressure
PEF	:	Photoelectric Factor
RQI	:	Rock Quality Index
SACROC	:	Scurry Area Canyon Reef Operators Committee
STB	:	Stock Tank Barrel
TACC	:	Texas Advanced Computing Center
TOF	:	Time of Flight

References

Al-Qenae, K. J., & Al-Thaqafi, S. H. (2015, November). New Approach for the Classification of Rock Typing Using a New Technique for Iso-Pore Throat Lines in Winland's Plot. In SPE Annual Caspian Technical Conference & Exhibition. Society of Petroleum Engineers.

Amaefule, J. O., Altunbay, M., Tiab, D., Kersey, D. G., & Keelan, D. K. (1993, January). Enhanced reservoir description: using core and log data to identify hydraulic (flow) units and predict permeability in uncored intervals/wells. In SPE annual technical conference and exhibition. Society of Petroleum Engineers.

Archie, G. E. (1942). The electrical resistivity log as an aid in determining some reservoir characteristics. Transactions of the AIME, 146(01), 54-62.

Berg, C. F. (2012). Re-examining Archie's law: Conductance description by tortuosity and constriction. Physical Review E, 86(4), 046314.

Campbell, W. G. 1990. Form and Style in Thesis Writing, a Manual of Style. Chicago: The University of Chicago Press.

Chen, H., & Heidari, Z. (2016). Quantifying the directional connectivity of rock constituents and its impact on electrical resistivity of organic-rich mudrocks. Mathematical Geosciences, 48(3), 285-303.

Choquette, P. W., & Pray, L. C. (1970). Geologic nomenclature and classification of porosity in sedimentary carbonates. AAPG bulletin, 54(2), 207-250.

Clerke, E. A., Mueller, H. W., Phillips, E. C., Eyvazzadeh, R. Y., Jones, D. H., Ramamoorthy, R., & Srivastava, A. (2008). Application of Thomeer Hyperbolas to decode the pore systems, facies and reservoir properties of the Upper Jurassic Arab D Limestone, Ghawar field, Saudi Arabia: A "Rosetta Stone" approach. GeoArabia, 13(4), 113-160.

Dempster, A. P., Laird, N. M., & Rubin, D. B. (1977). Maximum likelihood from incomplete data via the EM algorithm. Journal of the royal statistical society. Series B (methodological), 1-38.

Dunham, R. J. (1962). Classification of carbonate rocks according to depositional textures.

Embry III, A. F., & Klovan, J. E. (1971). A late Devonian reef tract on northeastern Banks Island, NWT. Bulletin of Canadian Petroleum Geology, 19(4), 730-781.

Fang, Q., & Boas, D. A. (2009, June). Tetrahedral mesh generation from volumetric binary and grayscale images. In Biomedical Imaging: From Nano to Macro, 2009. ISBI'09. IEEE International Symposium on (pp. 1142-1145). Ieee.

Ferreira, F. C., Booth, R., Oliveira, R., Boyd, A., Bize-Forest, N., & Wahanik, H. (2015, October). Truncated Multi-Gaussian Pore-Throat-Size Decomposition and a New Universal J-Function for Rock Characterization of Complex Carbonate Reservoirs. In OTC Brasil. Offshore Technology Conference.

Fraley, C., & Raftery, A. E. (1998). How many clusters? Which clustering method? Answers via model-based cluster analysis. The computer journal, 41(8), 578-588.

Fraley, C., & Raftery, A. E. (2002). Model-based clustering, discriminant analysis, and density estimation. Journal of the American statistical Association, 97(458), 611-631.

Gan, G., Ma, C., & Wu, J. (2007). Data clustering: theory, algorithms, and applications. Society for Industrial and Applied Mathematics.

Gandhi, A., Torres-Verdín, C., Voss, B., Gabulle, J., & Seminario, F. (2010, June). Construction of reliable static and dynamic multi-layer petrophysical models in Camisea gas reservoirs, Peru. In SPWLA 51st Annual Logging Symposium. Society of Petrophysicists and Well-Log Analysts.

Gao, B., Wu, J., Chen, S., Kwak, H., & Funk, J. (2011, May). New method for predicting capillary pressure curves from NMR data in carbonate rocks. In SPWLA 52nd Annual Logging Symposium. Society of Petrophysicists and Well-Log Analysts.

Garcia, A. P., & Heidari, Z. (2016, September). Quantification of Directional Pore Network Connectivity and Rock Fabric and its Application in Enhanced Assessment of Hydrocarbon Reserves. In SPE Annual Technical Conference and Exhibition. Society of Petroleum Engineers.

Gomes, J. S., Ribeiro, M. T., Strohmenger, C. J., Naghban, S., & Kalam, M. Z. (2008, January). Carbonate reservoir rock typing-the link between geology and SCAL. In Abu Dhabi International Petroleum Exhibition and Conference. Society of Petroleum Engineers.

Gunter, G. W., Spain, D. R., Viro, E. J., Thomas, J. B., Potter, G., & Williams, J. (2014, September). Winland Pore Throat Prediction Method-A Proper Retrospect: New Examples from Carbonates and Complex Systems. In SPWLA 55th Annual Logging Symposium. Society of Petrophysicists and Well-Log Analysts.

Halkidi, M., Batistakis, Y., & Vazirgiannis, M. (2001). On clustering validation techniques. Journal of intelligent information systems, 17(2), 107-145.

Hastie, T., Tibshirani, R., & Friedman, J. (2009). Overview of supervised learning. In The elements of statistical learning (pp. 9-41). Springer New York. Chicago

Heidari, Z., Hamman, J. G., Day, P. I., Gorney, D. L., & Alfred, D. (2011, May). Assessment of movable gas saturation and rock typing based on the combined simulation of petrophysical borehole measurements. In SPWLA 52nd Annual Logging Symposium. Society of Petrophysicists and Well-Log Analysts.

Herrick, D. C., & Kennedy, W. D. (1994). Electrical efficiency—A pore geometric theory for interpreting the electrical properties of reservoir rocks. Geophysics, 59(6), 918-927.

Hook, J. R. (2003). An introduction to porosity. Petrophysics, 44(03).

Kerans, C. (2001). Stratigraphic and diagenetic controls on reservoir architecture of a non-reefal icehouse isolated platform—Sacroc unit. Horseshoe atoll, Texas (abs.): AAPG Bulletin, 85, 386-387.

Kozeny, J. (1927). Uber kapillare leitung der wasser in boden. Royal Academy of Science, Vienna, Proc. Class I, 136, 271-306.

Leverett, M. (1941). Capillary behavior in porous solids. Transactions of the AIME, 142(01), 152-169.

Lucia, F. J. (1983). Petrophysical parameters estimated from visual descriptions of carbonate rocks: a field classification of carbonate pore space. Journal of Petroleum Technology, 35(03), 629-637.

Lucia, F. J. (1995). Rock-fabric/petrophysical classification of carbonate pore space for reservoir characterization. AAPG bulletin, 79(9), 1275-1300.

Lucia, F. J. (2007). Carbonate reservoir characterization: an integrated approach. Springer Science & Business Media.

Mishra, P. K., Al-Harthy, A., Al-Kanderi, J. M., Al-Raisi, M., Al-Alawi, G., Alhashmi, S., & Turkey, S. (2012, January). Rock Typing and Characterization of Carbonate Reservoirs. In SPE Kuwait International Petroleum Conference and Exhibition. Society of Petroleum Engineers.

Moore, J. C., & Saffer, D. (2001). Updip limit of the seismogenic zone beneath the accretionary prism of southwest Japan: An effect of diagenetic to low-grade metamorphic processes and increasing effective stress. Geology, 29(2), 183-186.

Moya, C., Gunter, G. W., Mahadevan, J., & Wolgemuth, K. M. (2012, January). Quantification of Hydrocarbon Volume: An Example Using Rock Typing Methodology Applied in Cerro Negro Field, Eastern Venezuela Basin. In SPE Latin America and Caribbean Petroleum Engineering Conference. Society of Petroleum Engineers.

Murray, R. C. (1960). Origin of porosity in carbonate rocks. Journal of Sedimentary Research, 30(1).

Oyewole, E., Garcia, A. P., & Heidari, Z. (2016a). A New Method for Assessment of Directional Permeability and Conducting Pore Network Using Electric Conductance in Porous Media. In SPWLA 57th Annual Logging Symposium. Society of Petrophysicists and Well-Log Analysts.

Oyewole, E., Saneifar, M., & Heidari, Z. (2016b). Multiscale characterization of pore structure in carbonate formations: Application to the Scurry Area Canyon Reef Operators Committee Unit. Interpretation, 4(2), SF165-SF177.

Palabos, 2013, The Palabos software project:

http://www.palabos.org/documentation/tutorial/permeability.html

Peters, E. J. (2012). Advanced Petrophysics: Dispersion, interfacial phenomena (Vol. 2). Greenleaf Book Group.

Pittman, E. D. (1992). Relationship of porosity and permeability to various parameters derived from mercury injection-capillary pressure curves for sandstone (1). AAPG bulletin, 76(2), 191-198.

Purba, S. A., Garcia, A. P., & Heidari, Z. (2017). Improved Permeability Assessment Using Directional Rock Fabric Quantification. In AAPG Annual Convention and Exhibition.

Purba, S. A., Garcia, A. P., & Heidari, Z. (2017, June). New Method for Rock Classification in Carbonate Formations Using Well-Log-Based Rock Fabric Quantification. In SPWLA 58th Annual Logging Symposium. Society of Petrophysicists and Well-Log Analysts.

Read, J. F., & Horbury, A. D. (1993). Eustatic and Tectonic Controls on Porosity Evolution Beneath Sequence-Bounding Unconformities and Parasequence Disconformities on Carbonate Platforms: Chapter 11: DIAGENESIS, SEQUENCE STRATIGRAPHY, AND CHANGES IN RELATIVE SEA LEVEL.

Rebelle, M. (2014, November). Rock-typing In Carbonates: A Critical Review Of Clustering Methods. In Abu Dhabi International Petroleum Exhibition and Conference. Society of Petroleum Engineers.

Reeves, S. R. (2007). Demonstration of a novel, integrated, multi-scale procedure for high-resolution 3D reservoir characterization and improved CO2-EOR/sequestration management, SACROC Unit. Advanced Resources International, Incorporated.

Rose, W., & Bruce, W. A. (1949). Evaluation of capillary character in petroleum reservoir rock. Journal of Petroleum Technology, 1(05), 127-142.

Roth, V., Lange, T., Braun, M., & Buhmann, J. (2002, July). A resampling approach to cluster validation. In International conference on computational statistics (Vol. 15, pp. 123-128).

Saikia, P., Shanat, F., Ahmed, K., Choudhary, P., Ferdous, H., Ahmed, F., & Fournier, F. (2016, December). Integrated Rock-Typing Workflow in Shallow Unconventional Reservoir in Kuwait. In SPE Heavy Oil Conference and Exhibition. Society of Petroleum Engineers.

Salvador, S., & Chan, P. (2004, November). Determining the number of clusters/segments in hierarchical clustering/segmentation algorithms. In Tools with Artificial Intelligence, 2004. ICTAI 2004. 16th IEEE International Conference on (pp. 576-584). IEEE.

Saneifar, M., Aranibar, A., & Heidari, Z. (2014). Rock classification in the Haynesville Shale based on petrophysical and elastic properties estimated from well logs. Interpretation.

Saneifar, M., Heidari, Z., & Hill, A. D. (2015). Application of Conventional Well Logs To Characterize Spatial Heterogeneity in Carbonate Formations Required for Prediction of Acid-Fracture Conductivity. SPE Production & Operations, 30(03), 243-256.

Serra, O. T., & Abbott, H. T. (1982). The contribution of logging data to sedimentology and stratigraphy. Society of Petroleum Engineers Journal, 22(01), 117-131.

Sheikholeslami, G., Chatterjee, S., & Zhang, A. (1998, August). Wavecluster: A multi-resolution clustering approach for very large spatial databases. In VLDB (Vol. 98, pp. 428-439).

Skalinski, M., & Kenter, J. (2013). Pore typing workflow for complex carbonate systems. In Presentation at AAPG Annual Convention and Exhibition Pittsburgh Pennsylvania.

Skalinski, M., Kenter, J., & Jenkins, S. (2009, January). Rock type definition and pore type classification of a carbonate platform, Tengiz Field, Republic of Kazakhstan. In SPWLA 50th Annual Logging Symposium. Society of Petrophysicists and Well-Log Analysts.

Smyth, P. (1996, August). Clustering Using Monte Carlo Cross-Validation. In Kdd (Vol. 1, pp. 26-133).

Tang, H. (2008, January). Improved carbonate reservoir facies classification using artificial neural network method. In Canadian International Petroleum Conference. Petroleum Society of Canada.

Theologou, P. N., Skalinski, M., & Mallan, R. K. (2015, August). An MICP-Based Pore Typing Workflow–Core Scale to Log Scale. In SPWLA 56th Annual Logging Symposium. Society of Petrophysicists and Well-Log Analysts.

Thomeer, J. H. M. (1960). Introduction of a pore geometrical factor defined by the capillary pressure curve. Journal of Petroleum Technology, 12(03), 73-77.

Tibshirani, R., & Walther, G. (2005). Cluster validation by prediction strength. Journal of Computational and Graphical Statistics, 14(3), 511-528.

Tibshirani, R., Walther, G., & Hastie, T. (2001). Estimating the number of clusters in a data set via the gap statistic. Journal of the Royal Statistical Society: Series B (Statistical Methodology), 63(2), 411-423.

Turabian, K. L. 1987. A Manual for Writers of Term Papers, Theses, and Dissertations. 5th ed. Chicago: The University of Chicago Press.

Vashist, N., Dennis, R. N., Rajvanshi, A. K., Taneja, H. R., Walia, R. K., & Sharma, P. K. (1993, January). Reservoir Facies and Their Distribution in a Heterogeneous Carbonate Reservoir: An Integrated Approach. In SPE Annual Technical Conference and Exhibition. Society of Petroleum Engineers.

Wright, W. R. (2011). Pennsylvanian paleodepositional evolution of the greater Permian Basin, Texas and New Mexico: Depositional systems and hydrocarbon reservoir analysis. AAPG bulletin, 95(9), 1525-1555.

Weakliem, D. L. (1999). A critique of the Bayesian information criterion for model selection. Sociological Methods & Research, 27(3), 359-397.

Wempe, W., & Mavko, G. (2002). Effective porosity-total porosity model applied to fontainebleau sandstone. In SEG Technical Program Expanded Abstracts 2002 (pp. 1870-1872). Society of Exploration Geophysicists.

Winsauer, W. O., Shearin Jr, H. M., Masson, P. H., & Williams, M. (1952). Resistivity of brine-saturated sands in relation to pore geometry. AAPG bulletin, 36(2), 253-277.

Wyllie, M. R. J., Gregory, A. R., & Gardner, L. W. (1956). Elastic wave velocities in heterogeneous and porous media. Geophysics, 21(1), 41-70.

Wyllie, M. R. J., & Rose, W. D. (1950). Some theoretical considerations related to the quantitative evaluation of the physical characteristics of reservoir rock from electrical log data. Journal of Petroleum Technology, 2(04), 105-118.

Xu, C., & Torres-Verdín, C. (2013). Pore system characterization and petrophysical rock classification using a bimodal Gaussian density function. Mathematical Geosciences, 45(6), 753-771.

Xu, C., Heidari, Z., & Torres-Verdin, C. (2012, January). Rock classification in carbonate reservoirs based on static and dynamic petrophysical properties estimated from conventional well logs. In SPE Annual Technical Conference and Exhibition. Society of Petroleum Engineers.